



HAL
open science

Experimental and numerical upscaling of foam flow in highly permeable porous media

Sagyn Omirbekov, Hossein Davarzani, Stéfan Colombano, Azita Ahmadi-Senichault

► **To cite this version:**

Sagyn Omirbekov, Hossein Davarzani, Stéfan Colombano, Azita Ahmadi-Senichault. Experimental and numerical upscaling of foam flow in highly permeable porous media. *Advances in Water Resources*, 2020, 146, pp.103761. 10.1016/j.advwatres.2020.103761 . hal-03005274

HAL Id: hal-03005274

<https://brgm.hal.science/hal-03005274>

Submitted on 17 Nov 2020

HAL is a multi-disciplinary open access archive for the deposit and dissemination of scientific research documents, whether they are published or not. The documents may come from teaching and research institutions in France or abroad, or from public or private research centers.

L'archive ouverte pluridisciplinaire **HAL**, est destinée au dépôt et à la diffusion de documents scientifiques de niveau recherche, publiés ou non, émanant des établissements d'enseignement et de recherche français ou étrangers, des laboratoires publics ou privés.

Experimental and numerical upscaling of foam flow in highly permeable porous media

Sagyn Omirbekov^{a,b}, Hossein Davarzani^{a,*}, Stéfan Colombano^a, Azita Ahmadi-Senichault^b

^a*BRGM (French Geological Survey), 3 Avenue Claude Guillemin, Orléans, 45100, France*

^b*Institut de Mécanique et Ingénierie de Bordeaux (I2M, TREFLE), Arts et Métiers ParisTech, Talence, 33405, France*

* Corresponding Author

Email Address: h.davarzani@brgm.fr

Tel: + 33 (0) 2 38 64 33 52

Address: 3, avenue Claude Guillemin, 45100 Orléans, FRANCE

Abstract

Foam in porous media has been studied as a tool for various applications. Recently, the technology has become relevant for contaminated-aquifer remediation, where porous media are highly permeable. Therefore, the behavior of foam flow in high permeability porous media still raises numerous questions. In particular, upscaling of the foam flow from pore to Darcy scale is still under debate. Since the behavior of bulk foam has been studied principally in the food and cosmetics industries, and foam flow in porous media has mainly been investigated in the oil industry, the link between bulk-foam behavior and foam flow in porous media is still missing. The upscaling of foam flow from the pore scale to the laboratory scale could give valuable insight for understanding foam flow in aquifers.

We studied the behavior of pre-generated foam with different foam qualities through the rheological characterization of bulk foam using a rheometer and also when flowing in a porous medium composed of 1 mm glass beads. Foam was formed by co-injecting surfactant solution and nitrogen gas through a porous column filled by fine sand. The homogenization method is used to study macroscopic foam flow properties in porous media by solving the non-linear boundary value problem. The rheology of bulk foam is then used as an input in the upscaling procedure for foam flow in different periodic model 2D and 3D unit cells.

From our experiments, we found that the bulk foam is a yield-stress fluid and that the yield-stress values increase with foam quality. Moreover, the rheology of bulk foam corresponds well to the yield stress (Herschel-Bulkley-Papanastasiou) model. We found that foam behaves as a continuous yield-stress fluid in highly permeable porous media. It was also shown that the apparent foam viscosity in porous media

increases with the foam quality at the same total flow rate. The results obtained from the rheometer successfully match the outcomes of apparent foam viscosity obtained by flow in porous media by a shifting parameter for the same foam quality. The apparent foam viscosity found in 1 mm glass-bead packing was much higher than bulk foam viscosity.

Experimental results were compared to numerical results on simple unit cells. Although we observed considerable differences between the experimental and numerical results of upscaling, the general trend was identical. The differences can be explained by the complexity of the foam flow in porous media, especially foam compressibility. We found that foam flow at low capillary numbers is influenced by the trapping effect and at high pressure gradients by the compressibility. Compressibility was estimated for foam flow in 1 mm glass-bead packing. When foam compressibility is insignificant, the upscaling model can predict foam-flow behavior well at the Darcy scale.

Keywords: bulk foam; porous media; rheology; non-Newtonian fluid; yield stress; upscaling

1. Introduction

Foam is a two-phase system where gas bubbles are dispersed in the continuous liquid phase. The liquid phase in foam is generally an aqueous surfactant solution that plays a crucial role in stabilizing the liquid films between bubbles by increasing the surface tension.

Foam is used in a wide variety of industrial applications due to its mechanical behavior combined with its sizeable specific area relative to the density (Prud'homme & Khan, 2017). For instance, foam in the oil industry can be used as a drilling fluid, as a mobility-control agent in enhanced oil recovery processes (Chen, et al., 2014), in matrix-acidization treatments (Rossen & Wang, 1999), and in gas-leakage prevention (Bernard & Holm, 1970). In soil remediation processes, foam can be used as a sweeping pollutant fluid (Hirasaki, et al., 1997), as fluid that transports soil-cleaning additives or gases (Maire, et al., 2019; Choi, et al., 2009). Moreover, in ordinary life foam can be found in many food and cosmetic products.

The mechanical behavior of bulk foam is complicated due to elastic, plastic, and viscous properties. Therefore, their complexity is analyzed using rheology (Coussot, 2005; Larson, 1999; Macosko, 1994). Many authors have experimentally studied the rheology of bulk foam in the last sixty years (Cohen-Addad, et al., 2013; Denkov, et al., 2009; Hohler & Cohen-Addad, 2005; Katgert, et al., 2013; Kraynik, 1988; Dollet & Raufaste, 2014; Khan, et al., 1988; Herzhaft, 1999; Denkov, et al., 2005). In most of the studies, bulk foam was identified as a yield-stress fluid and the majority of the results are commonly well fitted by the Herschel-Bulkley law. For instance, Khan et al. (1988) investigated bulk foam through a rheometer with parallel-plate geometry. The geometry was covered with sandpaper to eliminate the wall slip velocity. The average diameter of foam bubbles was 65 μm , as measured by an optical method. They demonstrated the existence of a yield stress for foams with 92%, 95% and 97% of gas fractions (f_g , foam quality), with the yield stress increasing with f_g .

A full understanding of foam flow in porous media is hindered due to the complex behavior of foam associated with the complex microstructure of porous media. There are also apparent contradictions in the conclusions of the studies on foam flow presented in the literature. For instance, some authors showed Newtonian (Persoff, et al., 1991) foam flow behavior in porous media, others shear-thinning (Hirasaki & Lawson, 1985; Falls, et al., 1989), a mixture of Newtonian and shear-thinning (Vassenden & Holt, 2000) or related to foam quality (Alvarez, et al., 2001). Hirasaki and Lawson (1985) reported non-linear behavior in foam when flowing through a smooth capillary tube and pointed out the impact of foam texture (bubble size) on apparent foam viscosity. Shear-thinning behavior of foam flow in homogenous bead packs was shown by Falls et al. (1989). Rossen and Wang (1999) modeled foam as a Bingham plastic flowing in sandstones. They assumed bubble size was fixed and roughly equal to pore size at low-quality regimes. Some authors also considered the presence of yield stress based on a threshold pressure gradient, which was linked with the types of gas and surfactant, surfactant concentration, and petrophysical properties of porous media (Rossen & Gauglitz, 1990; Dicksen, et al., 2002; Ransohoff &

Radke, 1988; Gauglitz, et al., 2002; Omirbekov, et al., 2020). However, in most of the foam modeling investigations in porous media, foam was characterized as a pure power-law fluid without assuming yield stress (Friedmann, et al., 1991; Kavscek, et al., 1997; Bertin, et al., 1998; Myers & Radke, 2000; Kam, 2008; Kavscek, et al., 2010; Ashoori, et al., 2012). Recently, Aranda et al. (2020) experimentally found the shear-thinning behavior of foam when studying the influence of permeability on the apparent foam viscosity in highly permeable porous media (Aranda, et al., 2020).

Several foam-modeling techniques have been developed since the 1980s, to understand and predict the complex behavior of foam flow in porous media (Ma, et al., 2015). Ma et al. (2015) provided a complete overview of existing methods for modeling foam in porous media. They categorized the modeling techniques into three groups depending on implicit or dynamic foam textures: local-equilibrium models, population-balance models, and others. They also indicated the possibility of using all models for direct incorporation into reservoir simulators based on material balance and Darcy law. They highlighted some studies on the upscaling of foam from laboratory-scale to field-scale in which the upscaling problems were pointed out due to entrance and end effects in laboratory core experiments.

On the other hand, a link between pore or bubble scale (discontinuous) physics and Darcy-scale (continuum) models is missing. This link is often ascertained through a variety of upscaling approaches (Berryman, 2005). For instance, Darcy's law is obtained from the creeping incompressible flow of a Newtonian fluid via the volume-averaging method with a no-slip boundary condition at the liquid-solid interfaces (Quintard & Whitaker, 1993; Quintard & Whitaker, 1994). In this method, intrinsic permeability is calculated as a function of closure variables for a given geometry (porous media) (Whitaker, 1999). However, upscaling is still a challenge for non-Newtonian fluids, which are described by non-linear partial differential equations. There are very few experimental, numerical, or analytical studies on the upscaling of the non-Newtonian fluids flow in porous media. Several authors theoretically/numerically investigated upscaling power-law fluids (Idris, et al., 2004; Wang, et al., 2014; Woods, et al., 2003; Orgéas, et al., 2006), viscoelastic fluids, yield-stress fluids, or considered the case of generalized non-Newtonian fluids (Orgéas, et al., 2007). Therefore, the upscaling of foam flow in porous media is still questionable (Ma, et al., 2015), especially in soil remediation, where the permeability of porous media is high. Some authors also empirically proposed a Darcy-scale equation for non-Newtonian fluids (Larry, et al., 1986; Chauveteau, 1982; Chevalier, et al., 2013; Rodríguez de Castro, 2019). Put simply, the extension of the Darcy scale equation for yield-stress fluid in anisotropic porous media is very complex and still open.

To our knowledge, the modeling of non-Newtonian fluids, especially yield-stress fluid flow in porous media, has received less attention due to strong coupling between the porous medium and the fluid's rheology. Most of the previous studies on foam in porous media were related to the oil industry, where bubble size was considered to be roughly equal to pore size. However, in soil remediation cases, the

porous medium is highly permeable and consists of large pores, and there the bubbles can be much smaller than the characteristic length in porous media.

Consequently, the main objective of this study was to show whether foam flow in highly permeable porous media can be deduced from the bulk foam behavior and if we can consider foam as a single-phase yield-stress fluid. We also aimed to characterize the rheological behavior of bulk foam experimentally and to scale-up analytically and numerically the foam flow from pore to laboratory-Darcy scale.

2. Theoretical considerations

One of the important characteristics of foam is its foam quality, which is the ratio of the injected gas volume to the total liquid and gas volume, and can be expressed as

$$f_g = \frac{Q_G}{Q_G + Q_L} \quad (1)$$

in which Q_G (mL/min) and Q_L (mL/min) are the volumetric gas and liquid flow rates, respectively. The sum of Q_G and Q_L provides the value of total flow rate Q . According to the value of gas fraction, bulk foam can be dry ($f_g > 99\%$), wet ($64\% < f_g < 99\%$), or considered as a bubbly liquid ($f_g < 64\%$) (Langevin, 2017). Moreover, foam bubble shape can be transformed from spherical to polyhedral by increasing the gas fraction (Kovscek & Radke, 1994). In porous media, Osterloh and Jante (1992) distinguished two particular foam flow regimes depending on foam quality in sand-pack experiments at a steady state. They found a low-quality regime (wet), in which the pressure gradient was constant regardless of the liquid flow rate, and a high-quality regime (dry), in which the pressure gradient was independent of the gas flow rate. A transition foam quality (f_g^*) divides these two regimes, and depends on porous media characteristics, types of surfactants, and gas (Alvarez, et al., 2001).

Newtonian-fluid flow in porous media can be considered as models of flow through a bundle of tortuous capillary tubes which have uniform radii, R . By the theory of Kozeny-Carman (Kozeny, 1927; Carman, 1997), tortuosity in capillaries is defined as the ratio between the effective length (L_{eff}), i.e. length of the tortuous capillaries and the lengths of equivalent straight capillary tubes (L). Hence, it was assumed that fluid entering into tortuous capillaries flows faster than the fluid flowing through the equivalent straight capillaries in order to reach to the end of the tube at the same time. Using this concept, flow in porous media can be presented as follows:

$$u = \frac{\emptyset R^2 \Delta P}{8\mu L} \left(\frac{L}{L_{eff}}\right)^2 \quad (2)$$

u (m/s) and ΔP (Pa) are Darcy velocity and pressure drop in the direction parallel to length L (m), μ (Pa.s) is the dynamic fluid viscosity, \emptyset is the porous media porosity. Eq. 2 is then identified with the Darcy velocity for the flow of Newtonian fluids in porous media (Darcy, 1856).

$$u = \frac{Q}{A} = \frac{K \Delta P}{\mu L} \quad (3)$$

where Q (m^3/s) and A (m^2) are the flow rate and cross-section surface area of the porous media. The mean pore radius could be calculated as the radius of straight capillaries composing a bundle giving the same flow:

$$R_{eq}^2 = \left(R \frac{L}{L_{eff}}\right)^2 = \frac{8K}{\phi} \quad (4)$$

In the preceding equation, R_{eq} (m) is the average pore throat radius, K (m^2) is the intrinsic permeability of the porous media. The term $\left(\frac{L}{L_{eff}}\right)^2$ represents the tortuosity in porous media. Hence, an equivalent shear rate ($\dot{\gamma}_{eq}$) for flow in porous media can be expressed as (Darby, et al., 2001),

$$\dot{\gamma}_{eq} = \frac{4\alpha u / \phi}{R_{eq}} \quad (5)$$

in which α is an empirical shift parameter associated with the bulk rheology of the fluid and the tortuosity of porous media (Chauveteau & Zaitoun, 1981). The tortuosity of packed spheres was assumed to be 25/12 from the derivation of the Blake-Kozeny equation using the capillary model (Christopher & Middleman, 1965; Hirasaki & Pope, 1974). As a consequence, Hirasaki and Pope (1974) proposed to use $\alpha \approx 0.69$ through $\alpha = 1/\sqrt{L/L_{eff}}$ for Newtonian fluids. Recently, Rodriguez de Castro (2019) experimentally found α equal to 0.68 in glass-bead packings.

If we consider Darcy's law as applicable for the flow of a non-Newtonian fluid in porous media, the effect of non-linear rheology of the fluid can be incorporated in the definition of an apparent viscosity given by

$$\mu_{app} = \frac{K \Delta P}{u L} \quad (6)$$

This apparent viscosity μ_{app} is not an intrinsic property of fluid and varies with the flow rate. It is a non-linear function of the equivalent shear rate given in Eq. (5), which can be varied relying on the flow rate. Moreover, the shear rate varies considerably as a function of the structure and the heterogeneity of porous media that change interstitial velocity.

The rheological behavior of yield-stress fluid for simple shear can be described through the Herschel-Bulkley model (Herschel & Bulkley, 1926):

$$\tau < \tau_0 \Rightarrow \dot{\gamma} = 0 \text{ (solid regime); } \tau > \tau_0 \Rightarrow \tau = \tau_0 + a\dot{\gamma}^n \text{ (liquid regime)} \quad (7)$$

where τ (Pa) is the shear stress, $\dot{\gamma}$ ($1/\text{s}$) is the shear rate, τ_0 (Pa) is the yield stress, a ($\text{Pa}\cdot\text{s}^n$), and n (-) are the consistency and flow indexes, respectively. The continuous, viscous model proposed by Papanastasiou (Papanastasiou, 1987) is used to prevent the main difficulty caused by the Herschel-Bulkley model in numerical studies due to discontinuous behavior at insufficient shear rates that tend the apparent viscosity to infinity. The Herschel-Bulkley-Papanastasiou (H-B-P) model can be written as follows:

$$\mu(\dot{\gamma}) = a(\dot{\gamma})^{n-1} + \frac{\tau_0}{\dot{\gamma}} [1 - \exp(-m\dot{\gamma})] \quad (8)$$

in which m (s) is the exponent index.

Denkov et al. (2005) studied foam rheology and wall slip velocity with 90% gas fraction using a rheometer. The foam used was generated using a syringe with a needle with id (inner diameter) of 2.5 mm. They found the power-law index equal to 0.25 and 0.42 for tangentially mobile and immobile bubble surfaces, respectively. Denkov et al. (2009) studied the effects of surfactant type and bubble surfaces on bulk foam rheology with $f_g \geq 80\%$. They classified the rheological behavior of foam into two different classes depending on values of power-law index n , by taking into account the viscous friction between bubbles and also between bubbles and solid walls, qualitatively. The results with $n \approx 0.5$ referred to the first system, which was described as the dominant friction in foam films, and the second type $n < 0.5$ (mostly between 0.2 and 0.25) was defined as the essential energy dissipation on the bubble surfaces. These studies show solid, plastic or viscoelastic behavior of foam below yield stress and non-Newtonian liquid regime above the yield stress. The transition from solid-like to liquid-like mechanical behavior is called yielding. The yielding can be explained through the complex shear modulus that appears at the transition from a mostly elastic regime where G' (Storage modulus) $>$ G'' (Loss modulus) towards predominantly viscous behavior $G' < G''$ (Larson, 1999). The behavior of inverse transition from liquid-like to solid-like is called jamming, which was studied by slightly decreasing the shear rates and measuring the stress (Liu & Nagel, 1998). The apparent viscosity of foam is several times larger than the viscosity of the continuous liquid phase, even at low shear rates. This can be explained from a description of foam at the molecular and bubble scale (Hohler & Cohen-Addad, 2005).

3. Experimental approach

Here we present the fluids and materials used. The experimental setups and procedures were provided to characterize the rheology of foam in bulk form and in porous media.

3.1. Fluids and materials

Surfactant solution

C₁₄₋₁₆ Alpha-olefin sulfonate (AOS) based surfactant Rhodacal® LSS-40/AX (Solvay Novecare) and demineralized/degassed water were used to prepare a surfactant solution. The surfactant contained 40 wt% of active materials in the aqueous solution. The chemical surfactant was chosen on the basis of several factors like soil biodegradability (Tuvell, et al., 1978; Talmage, 1994), market accessibility (Cserháti, et al., 2002), and field tests for soil remediation purposes (Svab, et al., 2009). The critical micelle concentration (CMC) of the surfactant is 1.8 ± 0.1 g/L, which is measured by the pendant-drop method (Stauffer, 1965) using a drop shape analyzer (DSA-100S, KRUSS). The surfactant solution was prepared at a concentration of four times CMC to avoid adsorption (Paria, 2008; Omirbekov, et al., 2020; Aranda, et al., 2020) at low concentrations and respect the biodegradability at high concentrations.

Gas

The gas used to generate foam in all experiments was nitrogen, provided by Air Liquide, with a purity of 99.98%. N₂ was selected after considering several studies presented in the literature, including foam stability (Farajzadeh, et al., 2009; Zeng, et al., 2016) and solubility (Sander, 1999) of gases. Also, carbon dioxide (purity > 99.7%), provided by Air Liquide, is used for pre-saturation procedures to avoid trapping of gas bubbles.

Porous media

Unconsolidated porous media made from calibrated silica sand (BR-37) and 1 mm glass beads are used, which are provided by Sibelco™ and Sigma-Aldrich companies, respectively. The sand-grading characteristics were as follows: the uniformity coefficient (C_u) is 0.72, the curvature coefficient (C_c) is 0.98; the effective size (d₁₀) and mean grain size (d₅₀) are 0.180 and 0.135 mm, respectively. Fine-sand packing was used to generate foam, while foam flow was examined in 1 mm glass-bead (GB) packing. The characteristics of the porous media are presented in Table 1.

Table 1 Properties of porous media

Porous media	Mean grain size diameter, d (mm)	Pore Volume, PV (mL)	Porosity, ϕ (%)	Permeability, K (m ²)	Mean pore radius, R_{eq} (μ m)
Sand BR37	0.135	51±2	38±1	7.2 (±1)×10 ⁻¹²	11.5
GB	1	181±2	36±1	8.30 (±0.1)×10 ⁻¹⁰	133.5

3.2. Experimental setups

The setups used to conduct the experiments are shown in Fig. 1. To generate foam, N₂ and the surfactant solution were co-injected into the foam generator column. Then the rheology of pre-generated foam was studied with different methods: A) in bulk form using a rheometer (bulk); B) in the main porous media column (p.m.).

The mass flow controller El-Flow Select F-201CV (Bronkhorst), providing a range of 0.16-10 mL_n/min (±0.5 % reading, plus ±0.1 % full scale), was used to control the gas flow rate and ensure the flow stability from a gas bottle. A piston pump Model 1HM (Eldex), with a precision of ±0.3 %, was used to inject the surfactant solution at a constant flow rate. The foam generator column was 10 cm long, with 4 cm inside diameter, and made of transparent polyvinyl chloride (PVC). The sand-pack was retained using a metallic grid with 42 μ m cell size. The following setups were used to investigate the pre-generated foam properties.

A) A rotational rheometer Haake Mars 60, Thermofisher (min. torque rotation $0.02 \mu\text{Nm}$, torque resolution 0.1 nNm) with serrated parallel plate geometry (P60/Ti/SE and TMP60/SE) was used to examine the rheology of pre-generated foam in bulk form.

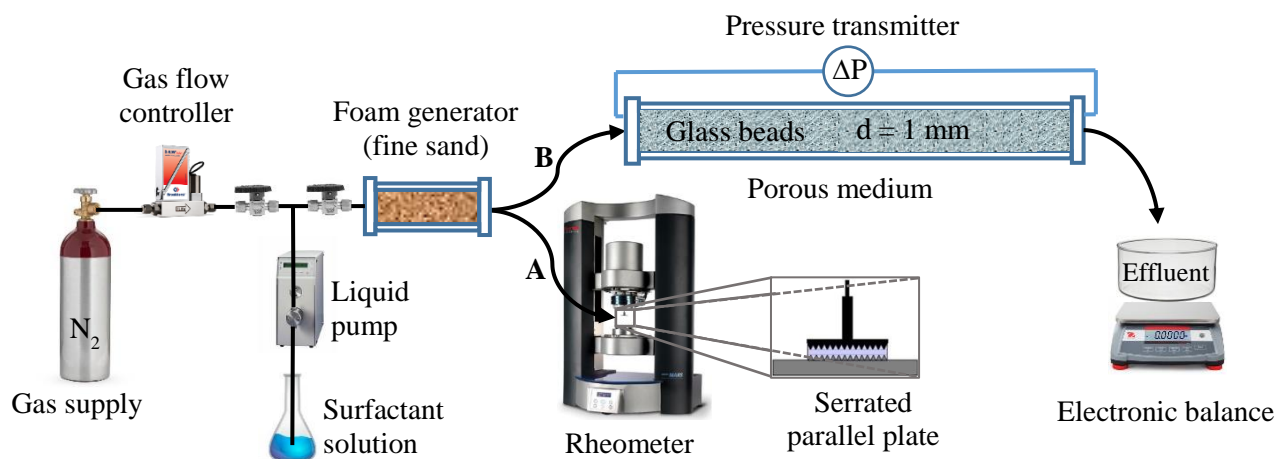


*Fig. 1 Schematic of the experimental setups used to characterize the rheology of
A) bulk foam and B) foam in porous media*

B) The main column (made of PVC material) with a length of 40 cm and an inner diameter of 4 cm packed by 1 mm glass beads was used to study foam from the foam generator column. Metallic grids with $150 \mu\text{m}$ cell size were used on each side of the column to contain the glass-bead packing. Pressure drop along the main column was measured through a differential pressure transmitter Rosemount 2051 (Emerson) with a 0-2500 mbar range (± 7 mbar at the maximum value). An electronic balance model STX 6201 (OHAUS) with a precision of 0.1 g was used to measure the effluent weight. The maximum pressure limit of the experimental installation was up to 6 bars controlled by the pump pressure sensor.

3.3. Experimental procedures

First, the porous columns were carefully packed and checked for leaks. The columns were flushed by CO_2 gas to remove any air. Then, degassed/demineralized water was injected into the columns, in a vertical position, with a 0.5 mL/min for at least five pore volumes (PV) to dissolve any CO_2 and thus to saturate the column thoroughly. As CO_2 is highly soluble in the water, this step was used to provide 100% of porous media saturation. To measure pore volume and porosity, the columns were weighed before and after the water saturation. The subsequent experimental steps were carried out with the column in a horizontal position. The permeability of the porous media was measured through the injection of degassed water with different flow rates while measuring the pressure difference and calculated via Darcy's law (Eq. 3). The measured properties of porous media were tabulated in Table 1. Next, the column was flushed with 3 PV of surfactant solution to complete adsorption. Finally, to generate foam, the surfactant solution and the nitrogen gas were simultaneously injected into the foam generator. 5 PV of fluids was co-injected to obtain a stable pre-generated foam. The pre-generated foam was further investigated A) using the rheometer and B) in glass-bead packing.

A) Pre-generated foams with 60%, 85%, and 95% foam qualities, generated at the same total flow rates ($Q = 2 \text{ mL/min}$, $u = 2.65 \times 10^{-5} \text{ m/s}$), were investigated using the rheometer. The mechanical properties of foam were probed through the rheometer, considering previous studies (Larson, 1999; Macosko, 1994). The parallel-plate geometry with serrated surfaces was used to avoid wall-slip velocity (Herzhaft, 1999; Marze, et al., 2008; Princen & Kiss, 1989). The shear gap of the geometry was 1 mm, which was chosen by taking into account previous studies (Herzhaft, 1999). Moreover, before starting the experiments, the dynamic stability of the foam at each quality was verified, based on the study of (Khan, et al., 1988), by examining samples at a constant shear rate. The idea was to observe how long the foam could withstand at constant torque. The decrease in torque values indicates the change in the foam structure. The volume of 3.1 mL of the foam sample was set in the gap, and the experiments were run in triplicate for each foam quality.

B) Firstly, the pre-generated foam was connected to the main column to study the impact of f_g and to determine the transition foam quality (f_g^*). Foam with a fixed total flow rate (2 mL/min) was studied for various foam qualities (40%-99%). The fractions of gas and liquid injected were controlled by the mass flow controller and the pump. The foam flow experiments were examined through the flow rate and pressure drop measurements along the column. Consequently, the apparent foam viscosity was derived from Darcy's law (Eq. 3). After determining f_g^* , foam flow in 1 mm GB packing was investigated at low-quality regimes. Foam flow with $f_g = 60\%$, 85%, and 95% was studied for different total flow rates that were increased step by step from minimum ($Q = 0.2 \text{ mL/min}$, $u = 2.65 \times 10^{-6} \text{ m/s}$) to maximum ($Q = 2.2 \text{ mL/min}$, $u = 2.92 \times 10^{-5} \text{ m/s}$) technically possible values. Thus, 905 and 82 minutes were required to inject 1 PV of pre-generated foam through the main column at the minimum and maximum flow rates, respectively. Experiments were duplicated by at least a descending flow rate experience. At the same time, the electronic balance measured the liquid effluent to determine the change of surfactant solution saturation (S_w) inside the main column. All experiments were carried out at 20°C, controlled room temperature, and atmospheric pressure.

4. Theoretical approach: upscaling technique

Since the direct upscaling of foam flow from pore to laboratory scale is complex, we used upscaling technique to scale up foam flow by using the rheological data of bulk foam as an input. The objective was to examine whether foam-flow behavior in porous media can be predicted from its bulk behavior. For field application in aquifers, a second upscaling from laboratory to aquifer scale should be considered. That was beyond the scope of this study.

In order to numerically study the macroscopic behavior of foam flow, it was first necessary to establish the geometry of representative elementary volume (REV) to correspond to the porous media permeability obtained from the laboratory experiments. To do so, we solved the closure problem for creeping flow of steady-state Newtonian fluids developed through the volume-averaging method (Quintard & Whitaker, 1994; Whitaker, 1999) to define the permeability of the two-dimensional (2D) and three-dimensional (3D)

unit cells (see Fig. 3). The size of solid inclusion in each kind of unit cell was adjusted to obtain the same permeability as in the 1D column experiment. Then the boundary value problem developed using the homogenization method (Auriault, 1991) was solved to study macroscopic foam-flow behavior further. The targets of the upscaling were to study the impact of f_g and the effect of different unit cell geometries on foam flow. Then the outcome of the 1D porous column experiments was used to correlate and validate the findings from upscaling.

4.1. Description of foam flow at the pore scale

The concept of porous media is presented in Fig. 2, in which we consider the foam flow through a periodic REV with Ω being the total volume of REV.

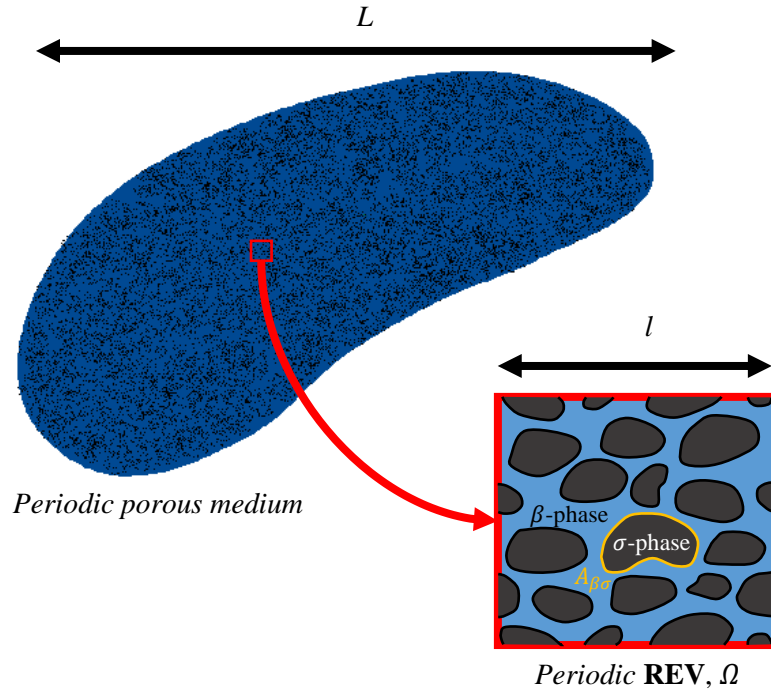


Fig. 2 A schematic illustration of a periodic porous medium with the associated REV

The volume considered consists of Ω_σ rigid solid-phase domain and the β yield-stress fluid (foam) of volume Ω_β . The porosity of the porous medium can be defined as $\phi = \Omega_\beta/\Omega$. A no-slip boundary condition is considered on the solid-fluid interface denoted $A_{\beta\sigma}$. Also, the fluid is considered as incompressible, purely viscous, and isotropic. Since the flow is in creeping regime (inertial effects are neglected) and steady-state, the mass and momentum balance equations for a yield-stress fluid are written as

$$0 = \nabla \cdot \left(-P\mathbf{I} + \mu(\dot{\gamma})(\nabla\mathbf{v} + (\nabla\mathbf{v})^T) \right) \quad \text{in } \Omega_\beta \quad (9)$$

$$\nabla \cdot \mathbf{v} = 0 \quad \text{in } \Omega_\beta \quad (10)$$

$$\mathbf{v} = 0 \quad \text{on } A_{\beta\sigma} \quad (11)$$

where \mathbf{v} is the fluid velocity field and P is the pressure. μ is the dynamic fluid viscosity, which can be defined by the H-B-P model (Eq. 8) for our case. Hence, the set of equations is the pore-scale description of the foam flow problem in highly permeable porous media.

4.2. Characteristics of the microstructure

Foam flow in model porous media was investigated with fixed permeability. The investigation was carried out in four different periodic 2D and two different 3D unit cells. The pore fraction (porosity) was adjusted to obtain the same permeability as the porous column permeability. The types of unit cells with their porosity values are presented in Fig. 3, with a) square-packed cylinders with a circular cross-section (SPC), b) square-packed cylinders with a square cross-section (SPS), c) close-packed cylinders with a circular cross-section (CPC), d) close-packed cylinders with a square cross-section (CPS), e) simple cubic packing of cubes (SCP), f) cubic body-centered packing of spheres (BCP).

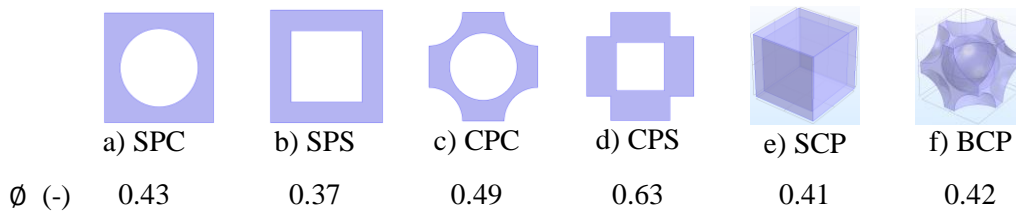


Fig. 3 2D and 3D periodic unit-cells for an array of parallel cylinders of circular (a, c), square (b, d) cross-sections, (e, f) simple cubic and cubic body-centered packings

The edge size of the periodic REV was selected to be 1 mm for all cases in order to be close to 1 mm GB size, and the permeability was set equal to $8.3 \times 10^{-10} \text{ m}^2$. The permeability of each porous medium has been calculated by solving the closure problem for Newtonian fluid flow through the volume-averaging method (Quintard & Whitaker, 1994; Whitaker, 1999). It should be noted that ideally, the unit cells chosen must have the same porosity and permeability as the experimental sample. Moreover, they should feature similar microstructures in terms of disorder. Although all unit cells considered here are ordered geometries, the porosity values for cells SPC, SPS, SCP and BCP are relatively close to each other and also close to the value found for the glass-bead packing. The porosity for CPC and CPS are significantly higher for the same value of the permeability.

4.3. Upscaling

Separation of scales

In order to meet the requirements of the homogenization method (Idris, et al., 2004; Orgéas, et al., 2007; Auriault, 1991; Papanicolau, et al., 1978; Sanchez-Palencia, 1980), the condition of separation of the scales must be satisfied for the porous media considered. As Fig. 2 describes, the characteristic REV length l is supposed to be small compared to the characteristic macroscopic length L , which can be expressed as

$$\epsilon = \frac{l}{L} \ll 1 \quad (12)$$

where ϵ represents the scale-separation parameter.

Boundary value problem

In this work, the homogenization procedure proposed by Orgeas (2007) has been used. Thus, a generalized Newtonian fluid through 2D and 3D elementary unit cells is studied using numerical simulations. To study foam flow in porous media, a boundary value problem concerning the first order velocity $\mathbf{v}^{(0)}$ also, to the second-order pressure $\nabla P^{(1)}$ is presented in the following way:

$$\nabla \cdot \left(-\epsilon P^{(1)} + \left(\frac{\tau_0}{|\dot{\gamma}|} [1 - \exp(-m|\dot{\gamma}|)] + a|\dot{\gamma}|^{n-1} \right) (\nabla \mathbf{v}^{(0)} + (\nabla \mathbf{v}^{(0)})^T) \right) = \nabla P_x^{(0)} \quad \text{in } \Omega_\beta \quad (13)$$

$$\nabla \cdot \mathbf{v}^{(0)} = 0 \quad \text{in } \Omega_\beta \quad (14)$$

$$\mathbf{v}^{(0)} = 0 \quad \text{on } A_{\beta\sigma} \quad (15)$$

Here, the unknowns $\epsilon P^{(1)}$ and $\mathbf{v}^{(0)}$ are periodic, and the macroscopic pressure gradient $\nabla P_x^{(0)}$ is given on the whole REV as a source term. Foam was considered as a yield-stress fluid following the rheological model H-B-P (Eq. 8), where the fluid viscosity is supposed to be a function of the magnitude of the shear rate $|\dot{\gamma}|$ given by

$$|\dot{\gamma}| = \sqrt{2\mathbf{S}:\mathbf{S}} \quad (16)$$

where the strain rate \mathbf{S} is defined as a function of the velocity field \mathbf{v} at the pore scale,

$$\mathbf{S} = \frac{1}{2} (\nabla \mathbf{v}^{(0)} + (\nabla \mathbf{v}^{(0)})^T) \quad (17)$$

The boundary value problem given above was solved in the 2D periodic unit-cell of circular cross-section (Fig. 3, a) for $f_g=60\%$, 85% and 95%, where the rheological parameters of the continuous, viscous model were obtained from the experimental study. Foam with $f_g=85\%$ was investigated in all geometries presented in Fig. 3. For all simulations in the ordered isotropic porous media, the macroscopic pressure gradient imposed $\nabla P_x^{(0)}$ was in the direction of the x-axis. The non-linear boundary value problem (Eqs. 13-15) was solved using Comsol Multiphysics Finite Element with a mixed pressure-velocity (P1-P2) formulation. The flow problems were solved through the Creeping flow module, which is designed for solving Stokes flow problems. The dynamic viscosity of the module was user-defined via the Equation View section. Solving this problem was similar to solving the direct flow problem in simple unit cells. The finite-triangular elements were used to mesh the 2D geometries. An example of mesh and boundary conditions used are in Fig. 4.

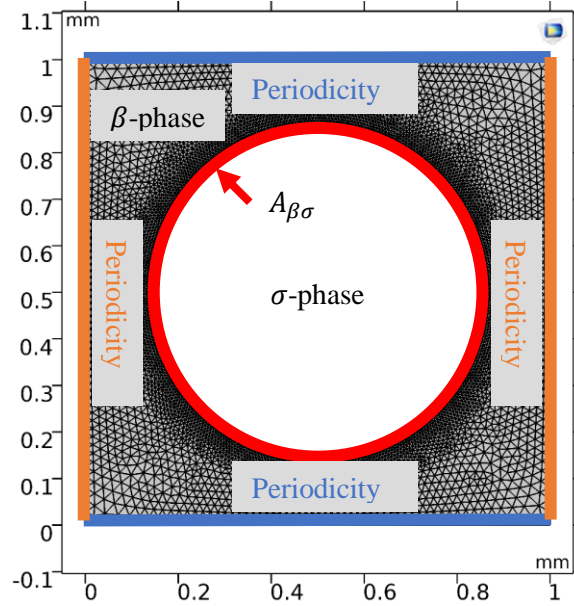


Fig. 4 The mesh and boundary conditions used to run the simulations

Results presented in the literature for the same geometries (Idris, et al., 2004; Orgéas, et al., 2007) were used to verify the numerical procedure adopted here in the case of power-law and generalized Newtonian fluids.

5. Results and discussion

5.1. Rheology of bulk foam

Fig. 5 shows the rheology of pre-generated foam for different foam qualities, in which the shear stress τ is displayed as a function of the shear rate $\dot{\gamma}$. The dots represent the average value of experimental results, and the lines describe the results of the H-B-P model. Table 2 shows the fitting parameters with coefficients of determination. The exponent index m was chosen to be 10000 in order to better represent the yield stress behavior in numerical studies. From these results, a non-Newtonian fluid behavior with yield stress is observed that was well fitted by the Herschel-Bulkley-Papanastasiou model. Moreover, we saw that yield stress increases with increasing foam quality thereby raising the bulk foam viscosity and the increasing yield-stress value with the foam quality, which agrees with the literature results (Khan, et al., 1988), where the storage modulus (G') and τ_0 as a function of foam quality (Marze, et al., 2009; Saint-Jalmes & Durian, 1999) were measured. The value of the yield stress increases by a factor 2 from $f_g=85\%$ to $f_g=95\%$, which can be explained by the evolution of the bubble shape from spherical to polyhedral-form, thereby increasing the friction between bubbles (Denkov, et al., 2009).

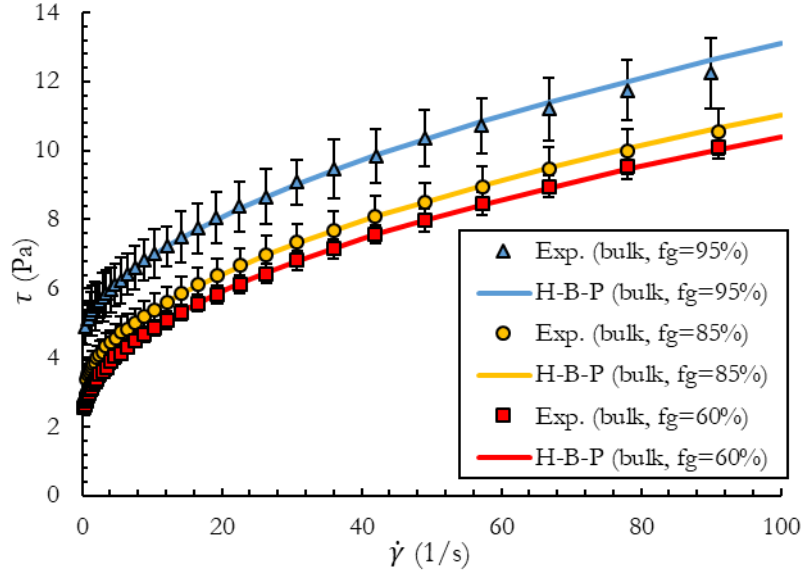


Fig. 5 Rheology of bulk foam with different foam quality

Table 2 Fitting parameters of H-B-P model

f_g (%)	60%	85%	95%
n (-)	0.48	0.52	0.54
τ_0 (Pa)	2.03	2.87	4.49
a (Pa.s ^{n})	0.94	0.76	0.7
m (s)	10000	10000	10000
R^2	0.99	0.99	0.99

It can therefore be concluded that in our experiments, bulk foam can be clearly considered as a yield-stress fluid. This is in agreement with previous studies in which the value of the flow index, n , obtained experimentally was indicated close to 0.5 (Denkov, et al., 2009; Marze, et al., 2008; Princen & Kiss, 1989; Ovarlez, et al., 2008; Ovarlez, et al., 2010; Tcholakova, et al., 2008).

It should be noted that the measurement of the rheology for the foam with the quality of $f_g=60\%$ was found to be complicated due to the drainage of foam liquid-phase from the rheometer geometry. Therefore, to avoid the liquid draining from the plates, we loaded the exact necessary amount of the foam sample (3.1 mL) by setting the gap to 3 mm, where the foam sample was placed between two plates. Then, the gap was decreased slowly until 1 mm to perform tests at different shear rates. The foam with the quality of $f_g=60\%$ was studied with great care at each shear rate by performing additional experiments to ensure accurate results.

These results are analyzed with the outcomes of the experimental study on porous media and further used as inputs for upscaling of foam flow in highly permeable porous media by considering foam as a yield-stress fluid.

5.2. Rheology of foam in porous media (Darcy scale)

Since foam was generated in the sand-pack, foam bubble size was expected to be smaller than the pore size of the glass-bead packing. Therefore, the bubble sizes were estimated according to previous studies. For instance, Marsden et al. (1967) noted that some foams generated in porous media could flow with bubbles much smaller than pores, as well as a series of foam films of various sizes, shapes, and configurations depending on the medium. They studied a pre-generated foam through the series of four identical porous media consisting of sand with a porosity of 35% and a permeability of 5.2 d. The foam texture was studied through optical cells and using a microscope. They showed an increase in bubble size with a decrease in foam mobility (the ratio of effective permeability to apparent viscosity). However, in later work, the opposite was revealed (Hirasaki & Lawson, 1985; Falls, et al., 1989). From the results of Marsden et al. (1967), we observed that the bubble size was smaller at high flow rates compared to the pore size, which was estimated to be five times smaller than the grain diameter.

Friedmann and Jensen (1986) found that the size of foam bubbles decreased with increasing velocities at constant foam quality by observing the texture of the foam exiting from several different porous media. Ettinger and Radke (1992) studied the foam texture of pre-generated foam in Berea sandstone. They also observed a decrease in bubble size with an increase in flow rate.

However, according to studies by Falls et al. (1989), the average size of the foam bubbles remained unchanged for the foam, which was pre-generated in 3 mm glass-bead packing and introduced into the second pack with the same grain size. The average size of the bubbles was estimated to be the same as the equivalent capillary radius of the packs. Consequently, in this study, we roughly assumed that the size of foam bubbles is equivalent to the pore size of the sand-pack (see Table 1).

The apparent foam viscosity calculated through Darcy's law (Eq. 6) applied to the experimental study of foam flow in the porous sample (1 mm glass-bead packing) as a function of foam quality is presented in Fig. 6. From these results, the transition foam quality (f_g^*) delimiting low and high-quality regimes is determined.

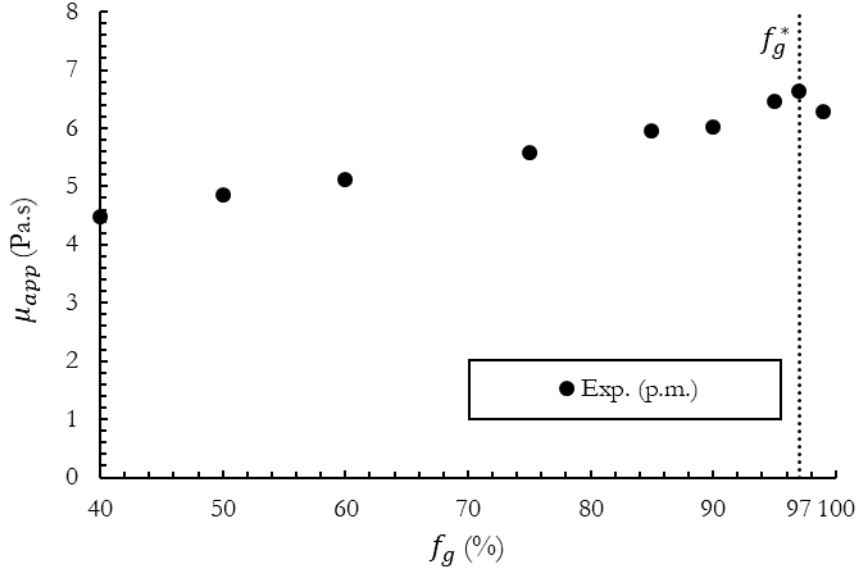


Fig. 6 Apparent foam viscosity in porous media (1 mm GB) as a function of foam quality at $Q=2$ mL/min

We observed that the transition foam quality was quite high and equal to 97% (dashed line). Hence, this result is in good agreement with the results of some authors (Alvarez, et al., 2001; Briceno & Joseph, 2003; Omirbekov, et al., 2020). For instance, Alvarez et al. (2001) found a value of $f_g^*=97\%$ for an experiment study of foam flow in a sand-pack with a permeability of 3.1 Darcy, where the foam was pre-generated through bronze wool (Alvarez, et al., 2001). They used two types of surfactants, an octyl ethoxylated alcohol and AOS, to generate foams. However, the bubble size of the pre-generated foam was not mentioned in their work.

Briceno and Joseph (2003) investigated pre-generated foam flow in a 1.2 m long channel (1 in. tall, 1/4 in. wide) and in a pipe (5/8 in. inner diameter). The foam was formed using an aqueous solution based on a mixture of AOS, polyacrylic acid polymer, cosurfactants (dodecanol), solvent (butanol), and water. They found $f_g^*=97\%$ through the pressure gradient vs. foam velocity plot where they discovered a shift in the results at $f_g>97\%$. It was also visually shown that there was a change in the structure of foam at this transition zone, in which foam flow behavior changed from uniform to slug flow.

Recently, Omirbekov et al. (2020) also found that transition-foam quality is independent of the porous-media grain size when the average foam-bubble size is smaller than the pore size of the porous medium. The value of transition-foam quality, for the same foam composition and pre-generated foam used in this study, was 97% for 2 mm, 4 mm, and 8 mm glass-bead packing. Nevertheless, the foam's bubble size can be changed depending on time. This is discussed in Appendix A. With these results in mind, all our further studies were chosen to be conducted in low-quality regime ($f_g=85\%$) to avoid the instability around f_g^* .

Fig. 7 shows the experimental results in terms of the pressure gradient along the porous column packed by 1 mm GB as a function of the foam flow velocity, for $f_g=60\%$, 85% , and 95% . Non-linear behavior was observed where the pressure gradient of flow increased with foam quality. We were unable to obtain ∇P values above foam injection flowrate of 3-4 mL/min due to the maximum pressure limit of the experimental configuration for $f_g=60\%$ and 85% of foams.

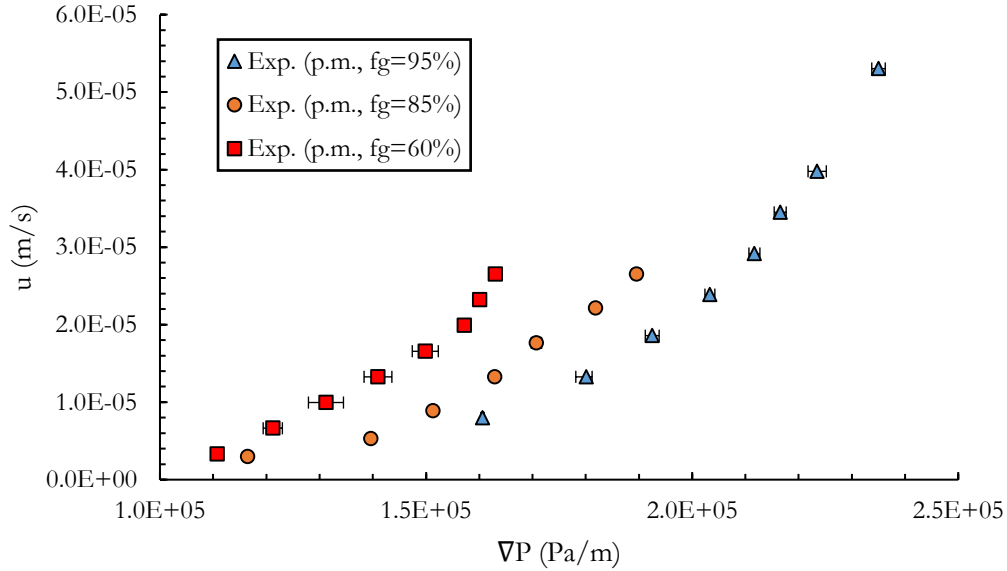


Fig. 7 The pressure gradient along the column as a function of the superficial velocity in GB, for $f_g=60\%$, 85% , 95%

To investigate the foam rheology, the apparent viscosity variations versus the equivalent shear rate (Eq. 5) were analyzed. The apparent foam viscosity as a function of the equivalent shear rate (Eq. 6) is plotted in Fig. 8, in which points represent experimental data, and the lines correspond to the fitting curves by the H-B-P model. Results show that foams in porous media behave as non-Newtonian yield-stress fluids, and the apparent viscosity of foam increases with foam quality. Therefore, we found that foam flow in porous media behaved as a bulk foam if the bubbles were smaller than the pore size and for a low-quality foam-flow regime. In addition, we observed that the yield-stress values for foams in porous media were about twice as high as those found for bulk foams (see Table 3). Moreover, the fluidity index n increased when the gas fractions decreased and had a value of 0.65 for $f_g=60\%$. In the literature, $n>0.5$ is found for low-quality bulk foams ($f_g<75\%$) (Otsubo & Prud'homme, 1994; Otsubo & Prud'homme, 1994; Larmignat, et al., 2008), so it agrees with our results. However, note that the power-law index n was around 0.5 for all bulk foams. This may be a consequence of the surface roughness since our porous medium consisted of glass-bead packing, and the pore walls are smooth compared to the serrated geometry of the rheometer. Also, it may be a result of the enduring sample preparation time for the foam with the quality of $f_g=60\%$ mentioned in section 5.1. Consequently, the foams can be classified into two

groups depending on foam quality and values of the power-law index, where we observed $n \approx 0.5$ for $f_g = 85\%$ and 95% and $n > 0.5$ for $f_g = 60\%$ foams.

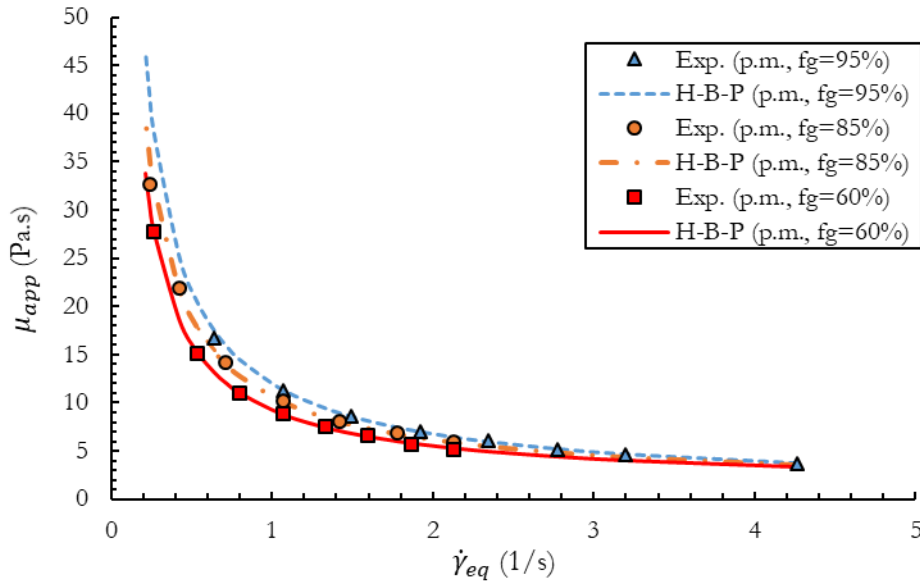


Fig. 8 Apparent viscosity as a function of the equivalent shear rate: $f_g = 60\%$, 85% and 95%

Table 3 Fitting parameters for H-B-P model

f_g (%)	60%	85%	95%
n (-)	0.65	0.53	0.49
τ_0 (Pa)	6.05	6.86	8.06
α (Pa.s ⁿ)	3.15	3.88	3.90
m (s)	10000	10000	10000
R^2	0.99	0.99	0.99

In Fig. 9a, the apparent viscosity of the bulk foam defined as $\tau/\dot{\gamma}$ is plotted as a function of shear rate for various foam qualities on a log-log scale. The apparent viscosity obtained from experiments in porous media is also presented in the same figure. The range of the shear rate was restricted in order to facilitate the comparison of the results. Fig. 9b shows the fitted results with the shift parameter α for each foam quality (Eq. 5). In this figure, the colored dots represent the outcomes of foam flow in porous media, and star dots are the result of the bulk foam examined through the rheometer. The fitted shift parameters α with the coefficient of determination are tabulated in Table 4 for each foam quality. Here, the shift parameter is found to allow a good superposition of the apparent viscosities of bulk and in-situ foam. Moreover, α becomes more significant with increasing foam quality. In previous studies related to yield-stress fluids, it was found that the shift parameter $\alpha > 1$ for sandstones (Fletcher, et al., 1991) and bead packings (Rodríguez de Castro, 2019; Zitha, et al., 1995). Also, α was mostly assumed to be constant and independent of flow rate. Recently, Rodriguez de Castro (2019) showed empirically, in glass-bead

packings, the dependence of α on flow rates where $\alpha > 1$ at slow flow rates and $\alpha < 1$ for high flow rates with a constant value at very high velocities (Rodríguez de Castro, 2019). However, note that all these studies were related to the flow of polymer solutions in porous media, and there is a lack of data for foams.

In this study, it was found that the values of α for foams are even smaller than those for Newtonian fluids in glass-bead packings (Rodríguez de Castro, 2019). Also, we observed that apparent in situ foam viscosity is higher than bulk foam viscosity at the same shear rate. Since bulk foam was examined at ambient conditions, this phenomenon may occur due to the effect of foam compressibility.

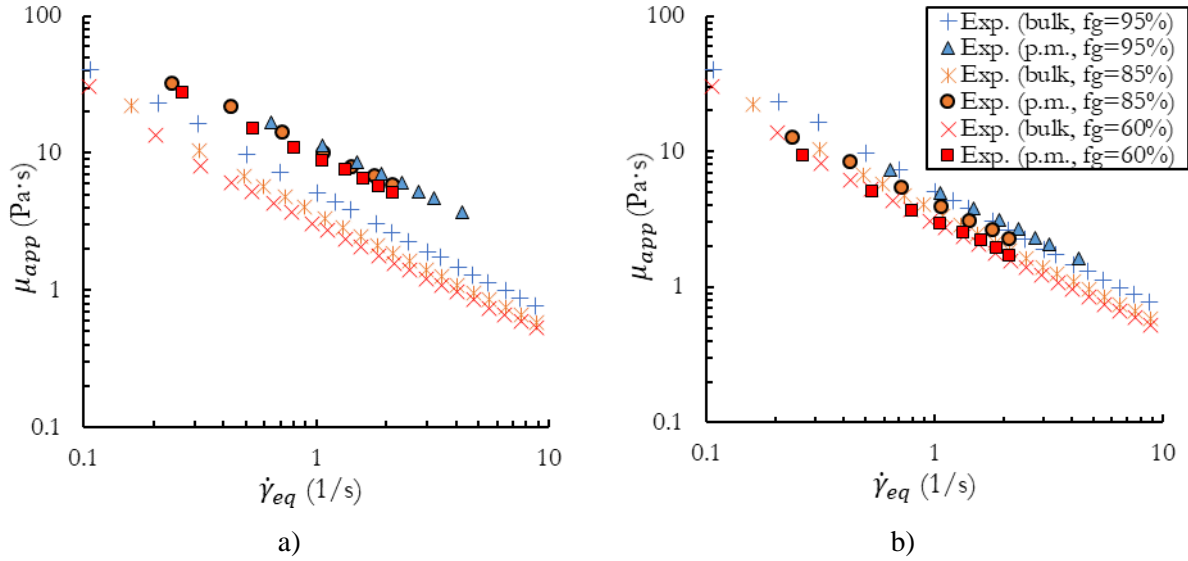


Fig. 9 Apparent viscosity vs shear rate a) experimental results b) fitted results with α shift parameter

Table 4 Shift parameter for various foam qualities obtained from 1 mm GB packing

GB size	1 mm		
f_g (%)	60%	85%	95%
α (-)	0.34	0.39	0.44
R^2	0.99	0.99	0.99

5.3. Upscaling of foam flow

5.3.1. Influence of foam quality

The outcome of the numerical study on foam flow in the periodic 2D SPC unit cell is compared to the experimental results in terms of the velocity/pressure gradient relationship in Fig. 10, for different foam qualities. In order to compare model results and experimental data, Fig. 10 was plotted on a semi-logarithmic scale. The dashed lines represent numerical results, in which the size of the solid cylinder was set in order to fit the experimental data in terms of permeability ($K=8.3 \times 10^{-10} \text{ m}^2$). The colored dots correspond to experimental results in 1 mm GB packing. Thus, the flow of foam with quality values of 60, 85, and 95% were examined to study the influence of foam quality on foam flow behavior. As experimental results, it is observed that the foam flow viscosity in porous media increases with f_g .

However, results from the numerical study show higher foam mobility even at lower pressure gradients compared to experimental results. The global trend of the curves and the behavior in terms of f_g follow the same tendency as those of the experimental results.

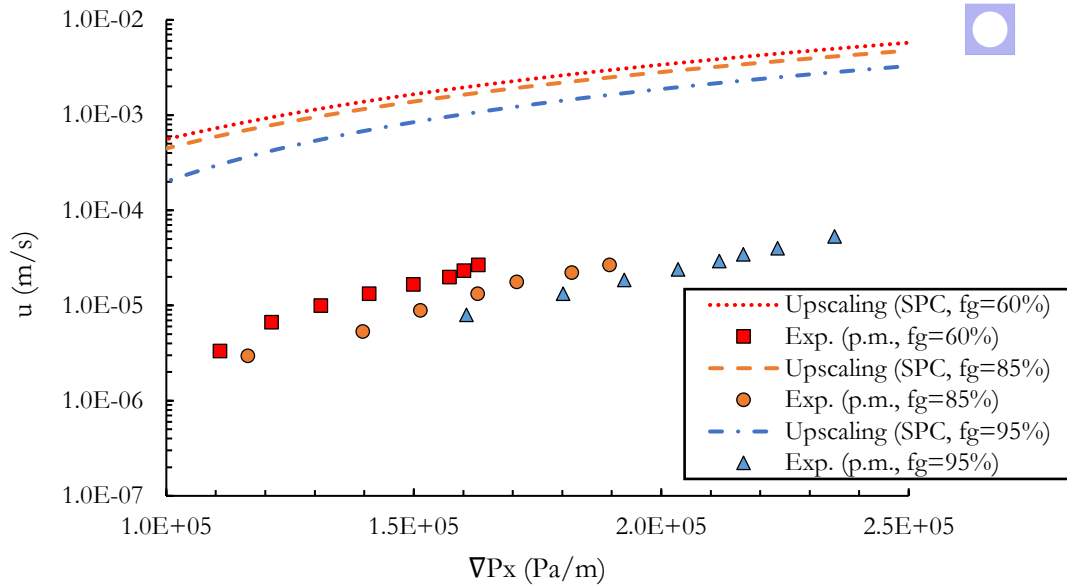


Fig. 10 Evaluation of the superficial velocity as a function of the macroscopic pressure gradient in 2D periodic SPC geometry, for different foam qualities ($f_g=60, 85$ and 95%)

5.3.2. Effect of porous media geometry

Fig. 11 shows the superficial velocity of foam as a function of the pressure gradient in different 2D and 3D geometries for $f_g=85\%$. The dashed lines correspond to the numerical results where the unit-cell geometry was adjusted to match the $K=8.3 \times 10^{-10} \text{ m}^2$ value in Newtonian case, and the colored dots represent the corresponding experimental results of GB packing for $f_g=85\%$

As Fig. 11 shows, the flow is non-linear and depends on the geometry of porous media, which plays a crucial role in the flow of yield stress fluids. Moreover, flow in 2D-SPC and 2D-SPS geometries are close to each other but differ from the outcomes of other unit cells. In addition, the results for more complex 2D unit cells CPC and CPS are very close to those of 3D unit cells SCP and BCP. Since the upscaling results were plotted on the semi-logarithmic scale, the small difference between the results was not explicitly shown. The porosity of 2D-SPC and 2D-CPS cells respectively equal 0.49 and 0.63, which is higher than the porosity of other unit cells where the values are close to 0.4. Therefore, we conclude that although the foam's behavior depends on the porous media structure. The results for the complex 2D and 3D geometries are closer to the experimental data than the simple 2D geometries. The predicted superficial foam velocities are however still a few order of magnitudes higher than the experimental data.

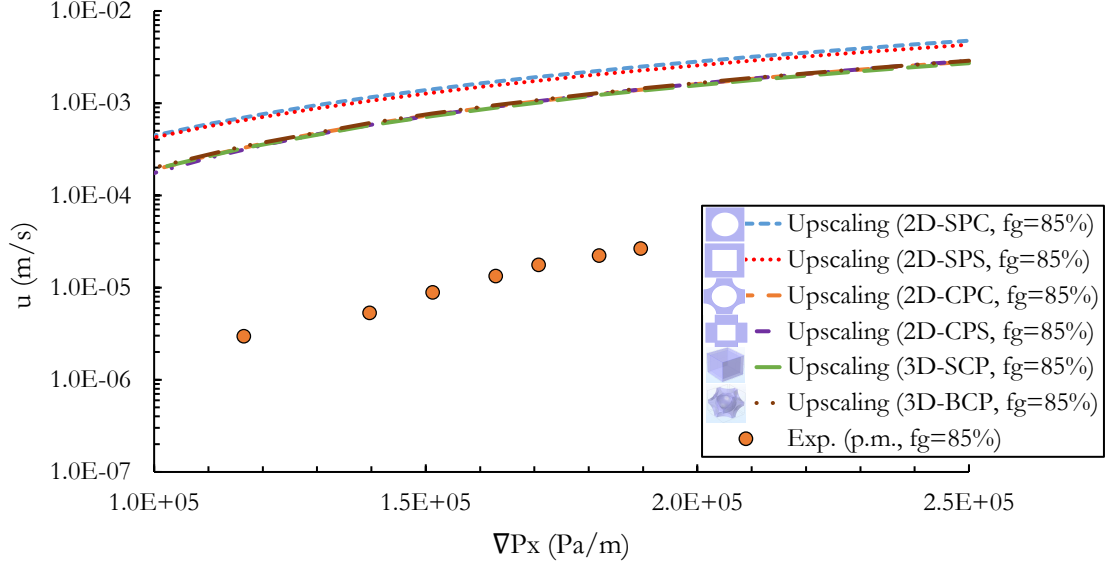


Fig. 11 The macroscopic pressure gradient vs. superficial velocity of foam flow in 2D SPC, SPS, CPC, CPS and 3D SCP, BCP unit cells ($f_g=85\%$)

This discrepancy can be attributed to the effects of compressibility and gas trapping, which should be considered during the study of foam flow in porous media.

To estimate the trapping effect in foam injection experiments, we calculated the capillary number N_{ca} using the following equation (Satter & Iqbal, 2015),

$$N_{ca} = \frac{KVP}{\gamma} \quad (18)$$

where $\gamma=0.036$ (N/m) is gas-liquid interfacial tension. Consequently, the capillary numbers as a function of pressure gradient can be written as $N_{ca} = 2.31 \times 10^{-8}\nabla P$. The minimum value of N_{ca} is then 2.55×10^{-3} which corresponds to our minimum measured pressure gradient (110782 Pa/m) where foam quality was 60%. This capillary number is even greater than the critical capillary number of 10^{-5} , above which the capillary forces become negligible according to several studies (Chatzis & Morrow, 1984; Ding & Kantzas, 2007). Therefore, gas trapping can be negligible in our experiments.

To better observe the effects of gas trapping and compressibility of foam with $f_g=85\%$ in the porous medium, we closed the outlet of the generator column and measured the pressure drop along the main column at the end of the experiment. From the result presented in Fig. 12, it is shown that the pressure in the column reduced gradually even after the foam supply was stopped. During the first two hours, the pressure gradient dropped sharply from 140,000 Pa/m to 37,000 Pa/m, after gradually decreasing, and the experiment lasted four days.

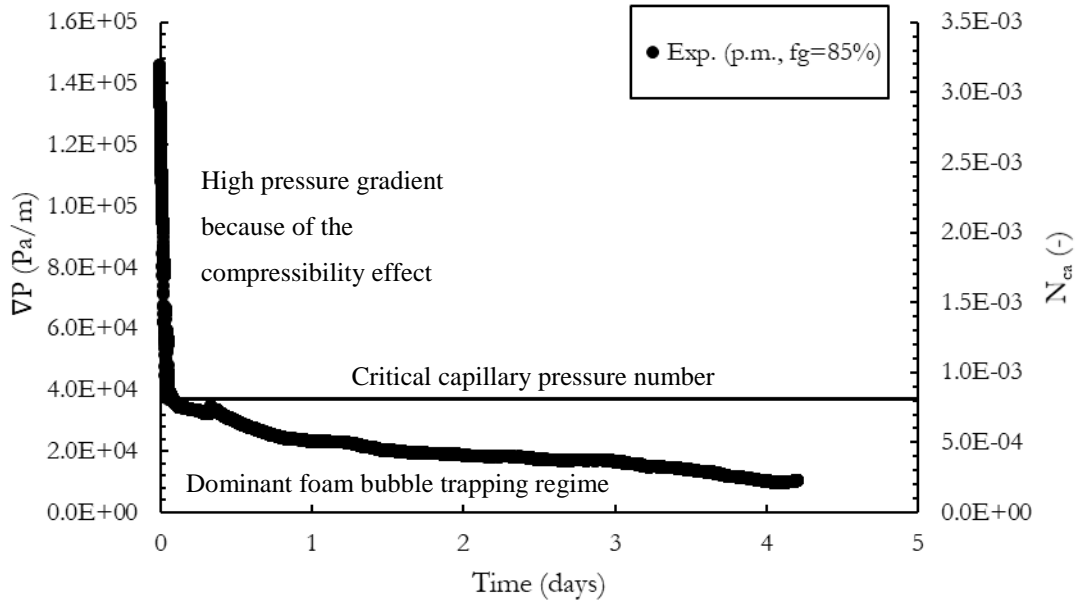


Fig. 12 Pressure gradient and capillary number as a function of time after the foam flow has stopped ($f_g=85\%$)

After closing the foam-generator outlet, foam continues flowing through the column. This can be explained by the foam compressibility effect. However, the pressure gradient falls first very fast and then more slowly because of the gas trapping. From the values of the capillary number shown in Fig. 12, we can say that the gas trapping occurs below a critical capillary-pressure number, $N_{ca}=7\times 10^{-4}$. This shows that our foam flow experiments in 1 mm glass-bead packing ($2.55\times 10^{-3}<N_{ca}<5.42\times 10^{-3}$) are not affected by the gas trapping.

We also observed the foam's compressibility and gas trapping effects by measuring the pressure gradient along the column and weighing the effluent. The pre-generated foam column was first connected to the GB column that was initially saturated by the surfactant solution. Fig. 13 shows a plot of the effluent mass and pressure gradient as a function of the main column PV. The PV of the GB packing was 180.9 mL, which is shown in Fig. 13 by the continuous black line. The total-injection rate into the foam generator was 2 mL/min, including 1.20 mL/min of N_2 gas and 0.80 mL/min of surfactant solution. However, the gas breakthrough happened after producing of 2.94 PV of liquid, which corresponds to a slope change in the figure (dotted black line). Hence, 2.94 times more liquid was recovered than initially stated in the column.

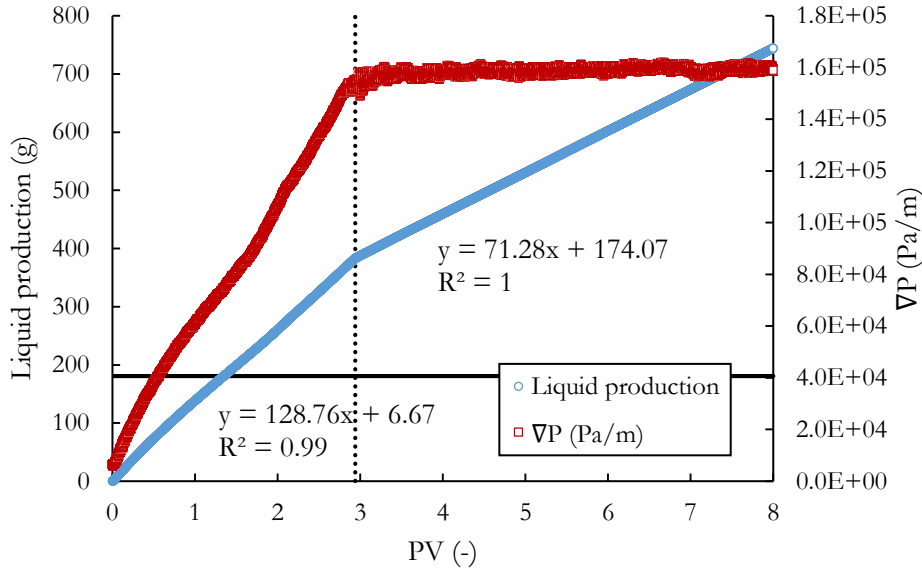


Fig. 13 Liquid mass of effluent as a function of PV for GB packing at $Q_t=2$ mL/min for $f_g=60\%$

This indicates compressibility and trapping of gas in porous media that delayed the gas breakthrough time. From Fig. 12, we discovered that the gas was trapped considerably below 37,000 Pa/m. Thus the liquid flowed within foam lamellae at the low pressure gradients. This phenomenon was also observed by Falls et al. (1989). They found the flow of foam lamellae through a single-flow path where stationary lamellae blocked most of the cross-sectional area of the bead-pack at sufficiently low pressure gradients. Since the gas was trapped in the porous medium, all liquids were transported through the lamellae, thus delaying the gas breakthrough. Therefore, we recovered 385 mL of liquid when the gas breakthrough occurred, that is, 2.1 times more than PV. Moreover, based on the trend equation of liquid production for the first half of the curve, the liquid recovery rate was approximately 128.8 mL per injected PV, which is 24% less than the injection volume (180.9 mL). If we consider that the liquid is an incompressible fluid, the volume of gas is reduced to 40%. Therefore, we can conclude that foam flow at low capillary numbers is influenced by the trapping effect and at high pressure gradients by the compressibility, which tends to decrease the foam's gas volume. After the breakthrough, when the foam had reached the column outlet, the change of effluent weight corresponded to the mass of the injected fluid. As a consequence of these results, foam compressibility must be taken into account during the study of foam rheology in confined media.

Since most of the foam volume is gas, compressibility is one of the essential parameters. The compressibility is often described in terms of the expansion ratio ε which is defined as the ratio between the density of liquid phase ρ_l and the foam density ρ_f ($\varepsilon=\rho_l/\rho_f$) (Valko & Economides, 1992). The expansion pressure should be determined for each pressure drop. Using the volume-equalization method proposed by (Valko & Economides, 1992), one should obtain a single master curve by plotting normalized-shear stress (τ/ε) versus normalized-shear rate ($\dot{\gamma}/\varepsilon$) regardless of the pressure and foam quality. According to Valko and Economides (1992), this method is relevant for low expansion foams

($\varepsilon < 4$) with spherical bubbles. Gardiner et al. (1999) highlighted an increase in apparent-foam viscosity with the expansion ratio by analyzing and fitting the foam-viscosity data from previous research. They also found that the volume-equalization method proposed by Valko and Economides (1992) is applicable to polyhedral ($\varepsilon > 5$) and bubbly-to-polyhedral ($5 \geq \varepsilon \geq 4$) foams (Gardiner, et al., 1998). Most of these studies were done using simple geometries such as pipes. Therefore, the determination of the expansion ratio in a porous medium is more difficult, if only the pressure drop along the column is measured.

To avoid the compressibility effect, we investigated the upscaling of foam flow in a more highly permeable porous medium based on the results of 4 mm glass-bead packing from Omirbekov et al. (2020). In this case, foam was pre-generated using the same surfactant solution and sand-pack. The maximum pressure gradient was 23,210 Pa/m at the flow rate of 3 mL/min at $f_g = 85\%$. Hence, the permeability of the unit cells was adjusted to the permeability of 4 mm glass-bead packing, $K = 1.09 \times 10^{-8} \text{ m}^2$. No gas trapping was expected as the capillary numbers were 4.5×10^{-3} and 7×10^{-3} at the flow rates of 0.22 and 3 mL/min, respectively. Fig. 14 shows the upscaling results through the different 2D and 3D geometries with the experimental outcomes from Omirbekov et al. (2020). In this case, the upscaling results are close to the experimental data.

Because the compressibility effect is insignificant in 4 mm glass-bead packing ($\varepsilon \cong 1$), we estimated the expansion ratio for 1 mm glass-bead packing using the volume equalization method of Valko and Economides (1992). In Fig. 15, we plotted the shear stress versus the shear rate of $f_g = 85\%$ foam in 1 mm glass-bead packings without and with mean-expansion factor, based on the 4 mm GB packing results. We found a mean-expansion factor of $\varepsilon = 2.1$ for 1 mm glass-bead packing. Because the bubble shape of the foam in porous media is more spherical, the method of Valko and Economides (1992) for low expansion foams is applicable.

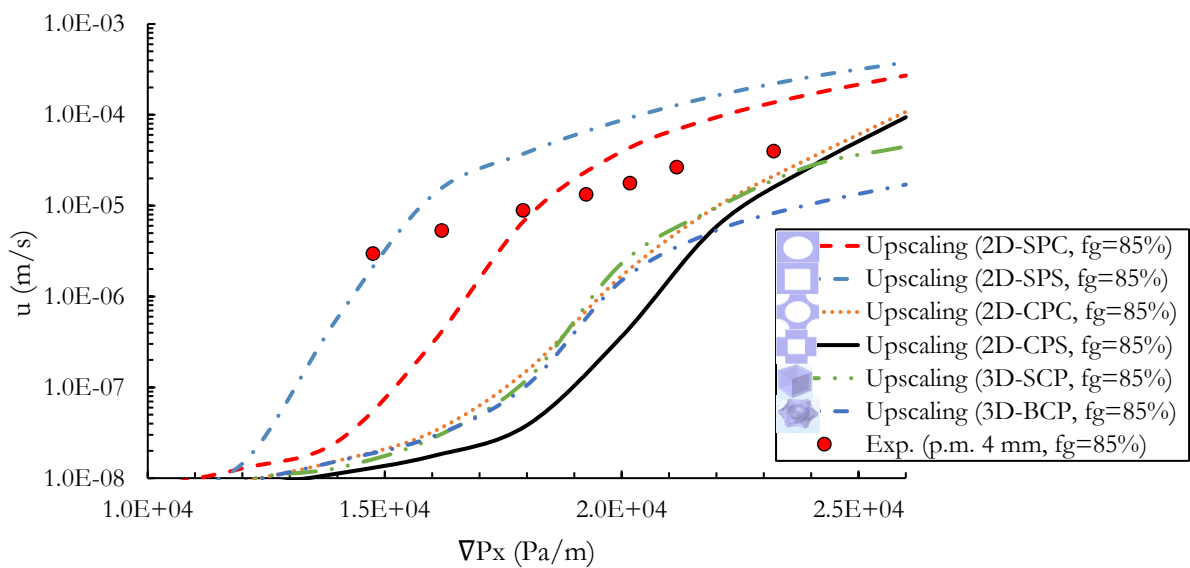


Fig. 14 The superficial velocity of foam flow vs. the macroscopic pressure gradient in 2D and 3D unit cells and experimental results in 4 mm GB packing of Omirbekov et al. 2020 ($f_g = 85\%$)

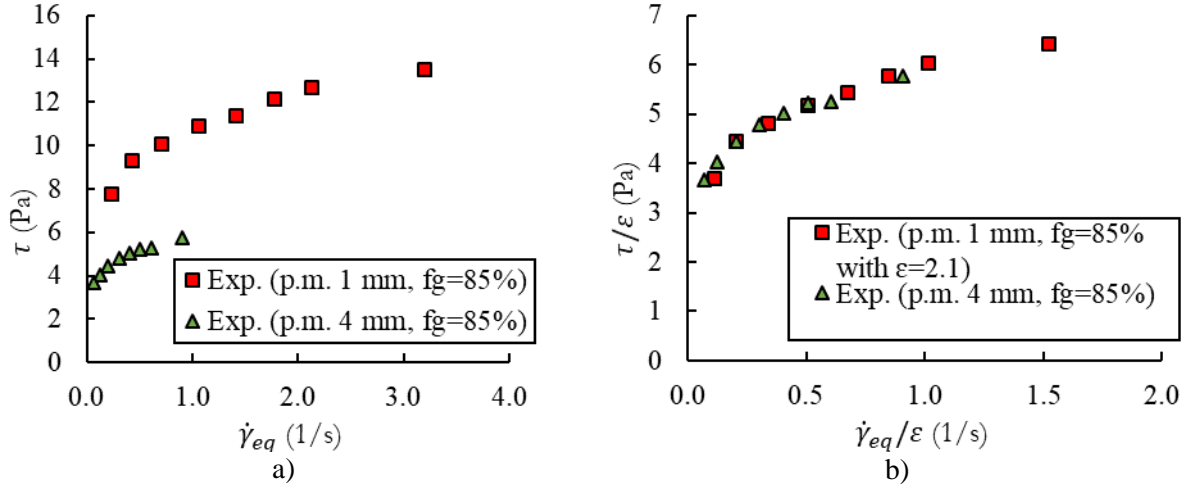


Fig. 15 Shear stress as a function of shear rate for foam quality of $f_g = 85\%$ in 1 and 4 mm GB packings
a) without expansion factor b) with $\varepsilon=2.1$ expansion factor for 1 mm GB packing

We note also the simplicity of the unit cells considered here where the pore-scale structure is highly ordered which may also influence the results and partly explain the discrepancies observed. Consequently, upscaling is an encouraging tool if the input parameters are settled by taking into account not only the real structure of the porous medium but also all phenomena involved for foam flow in confined media. In this paper, we only investigated the upscaling of foam flow from pore-scale to laboratory-scale. Therefore, the second upscaling from laboratory-scale to field-scale should be explored in the future. Then foam stability, including coalescence and gravity segregation, needs to be investigated. We know that in field applications, foam texture and bubble sizes may be different, as foam-residence time can be much longer.

5.3.3. Empirical Darcy-scale law

To further study foam flow in porous media using the bulk foam viscosity as input, we used the purely empirical approach of Chevalier et al. (2013) for the flow of yield-stress fluids (YSF) in glass-bead packings with a bead diameter d , which is presented in the following form (Chevalier, et al., 2013):

$$\nabla P = \frac{\chi\tau_0}{d} + \frac{\omega a \left(\frac{u}{d}\right)^n}{d} \quad (19)$$

They considered a polymer (Carbopol aqueous solution) and an emulsion (water-in-oil emulsion with a surfactant solution) as yield-stress fluids. In their study, the relationship between the pressure gradient (∇P) and the Darcy velocity (u) is of the same form as the constitutive law of the fluid, which contains the yielding term. In the preceding equation, terms χ and ω are dimensionless coefficients that depend on the distribution of shear rate intensity and on the power-law index (Chevalier, et al., 2014). To determine the dimensionless coefficients of YSF Darcy's law, we used the H-B-P fitting parameters of bulk foam and deduced χ and ω parameters by adjusting to $u(\nabla P)$ results of foam flow in GB packing. Fig. 16 presents the experimental results with the fitted YSF Darcy law, in which the colored dots represent the results of experiments through the GB packing and dotted lines are the results of the extended Darcy's

law for yield-stress fluids with fitted parameters. The corresponding dimensionless coefficients and coefficient of determination for each foam quality are presented in Table 5.

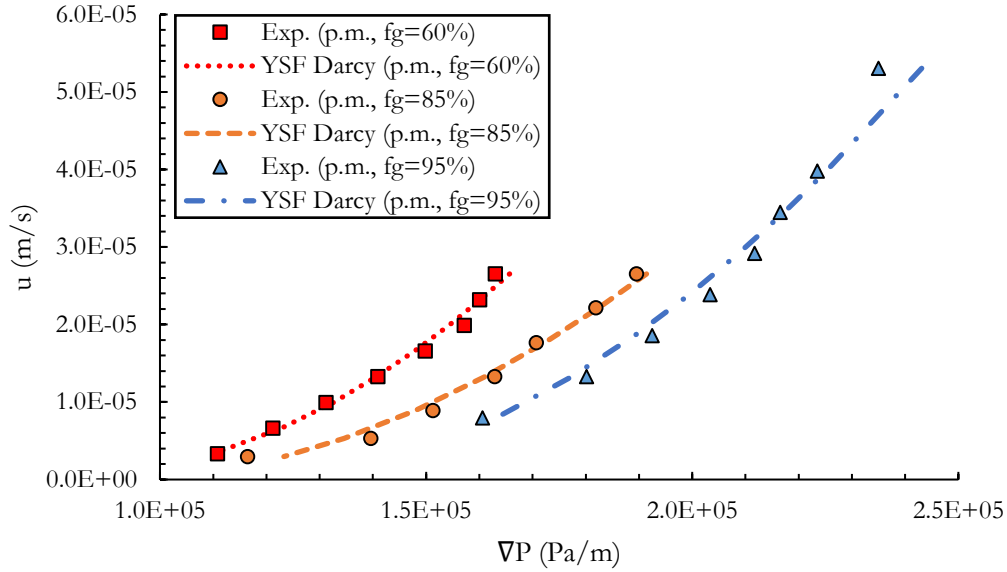


Fig. 16 Superficial velocity as a function of the pressure gradient for column experiments and the fitting curve by YSF Darcy's law for different foam qualities ($f_g=60\%$, 85% and 95%)

Table 5 The dimensionless coefficients determined for foams ($f_g=60\%$, 85% and 95%)

f_g (%)	60%	85%	95%
χ (-)	38.2	31.8	26.4
ω (-)	535.6	870	870
R^2	0.99	0.98	0.98

The values of the dimensionless coefficients determined are found to be very high in comparison to previous results of Chevalier et al. (2013, 2014) (Chevalier, et al., 2013; Chevalier, et al., 2014), in which they found χ equal to 12 and 5.5 for the polymer solution and for the water-in-oil emulsion, respectively. The dimensionless coefficient ω was 85 for both types of fluids.

Our results showed that χ decreases with increasing foam quality, and is 2-6 times higher than the values found for the polymer and the emulsion. Therefore, we recommend considering χ as a function depending on foam quality. Moreover, it was observed that the coefficient ω was 870 for foams with 85% and 95% foam qualities, but it was 535.6 for $f_g=60\%$. These results can be an outcome of power-law index values, which was high for $f_g=60\%$ foams. Thus in our case, ω should be considered individually for bubbly liquids ($f_g<64\%$), low-quality ($64\%\leq f_g\leq 97\%$) and high-quality foams ($f_g>97\%$).

Consequently, we can conclude that the Darcy-scale law depends on foam quality as foam rheology changes with the fraction of gas and liquid.

6. Conclusion

This work investigated the upscaling of foam flow for very high permeability porous media. The impact of foam quality on the apparent foam viscosity, with a fixed flow rate, was examined to distinguish the low and high-quality regimes. The rheology of pre-generated foam through the fine sand was studied as a bulk foam in a rheometer. Foams of different qualities were also injected into a porous column filled with 1 mm glass beads, from which the foam rheology was deduced. The results of both methods were fitted by a rheological model (Herschel-Bulkley-Papanastasiou model) and analyzed by comparison with each other. Foam flow's macroscopic behavior was also numerically studied in different periodic 2D and 3D unit cells by using the rheological data of bulk foam as an input. We also used the empirical Darcy scale law proposed by Chevalier et al. (2013) to derive dimensionless coefficients from our experimental results. We draw the following conclusions:

- Bulk-foam was found to behave as a yield stress fluid and the yield-stress values increased with foam quality. The rheological behavior of foam fits well with the Herschel-Bulkley model.
- Foam in highly permeable porous media ($K=8.3\times 10^{-10}\text{ m}^2$) was also found to behave as a yield-stress shear-thinning fluid regardless of the foam quality. It was also shown that the apparent foam viscosity in porous media increases with the foam quality at the same total flow rate.
- Apparent foam viscosity was seen to be 3-4 times higher than bulk foam viscosity at the same shear rate, which may be due to the complexity of the foam flow in porous media. However, this difference was smaller for very highly permeable porous media. Secondly, the values of dimensionless coefficients of empirical extended Darcy's law exhibited high values for foam compared to other yield-stress fluids and varied depending on foam quality.
- Considerable differences were observed in the experimental and numerical results of upscaling. The global trend of the curves and the behavior in terms of f_g followed the same tendency as those of the experimental results. The experimental results for a very highly permeable porous medium, where the compressibility effect is not significant, fitted well to the experimental data. In the absence of the foam trapping (e.g., a high capillary number), the difference between upscaling results and experimental data can be related to the foam compressibility. Therefore, foam rheological behavior in porous media can be easily predicted from the bulk foam in the case where the foam compressibility is negligible. The calculated compressibility coefficients should be increased with increasing pressure gradients.
- Upscaling can be an encouraging tool to predict foam-flow behavior from its bulk behavior. However, further investigations are necessary to incorporate the complex nature of the foam flow in porous media into the upscaling model. These insights are a promising point for studying foam flow in highly permeable porous media.

Acknowledgments

This study was performed as part of the “Famous” project. The authors would like to thank ADEME for co-funding the project under the “GESIPOL” program and Bolashaq International Scholarship from Kazakhstan government for providing the PhD grant for Sagyn Omirbekov. We gratefully acknowledge the financial support provided to the PIVOTS project by the “Région Centre – Val de Loire” and the European Regional Development Fund.

Appendix A

To study the variation of foam bubbles in bulk form (Fig. 1A a) and in 1 mm GB packing (Fig. 1A b), we used a dynamic foam analyzer (DFA-100, KRÜSS). The foam analyzer consists of a glass column (250 mm long and 40 mm internal diameter), a camera, and a light source. The experiments were conducted as in studies by Omirbekov et al. (2020), where N_2 gas was injected into the surfactant solution (AOS, $4 \times \text{CMC}$) using a porous-glass disc. The porous-glass disc was chosen according to the foam generator, where the pore size varied from 10 to 16 μm . In the porous medium, the used volumetric amount of the surfactant solution and the gas injection time were reduced by 60% since the porosity of the bead-pack was about 40%. In both cases, the camera height was set to 100 mm to record the change in bubble size over time.

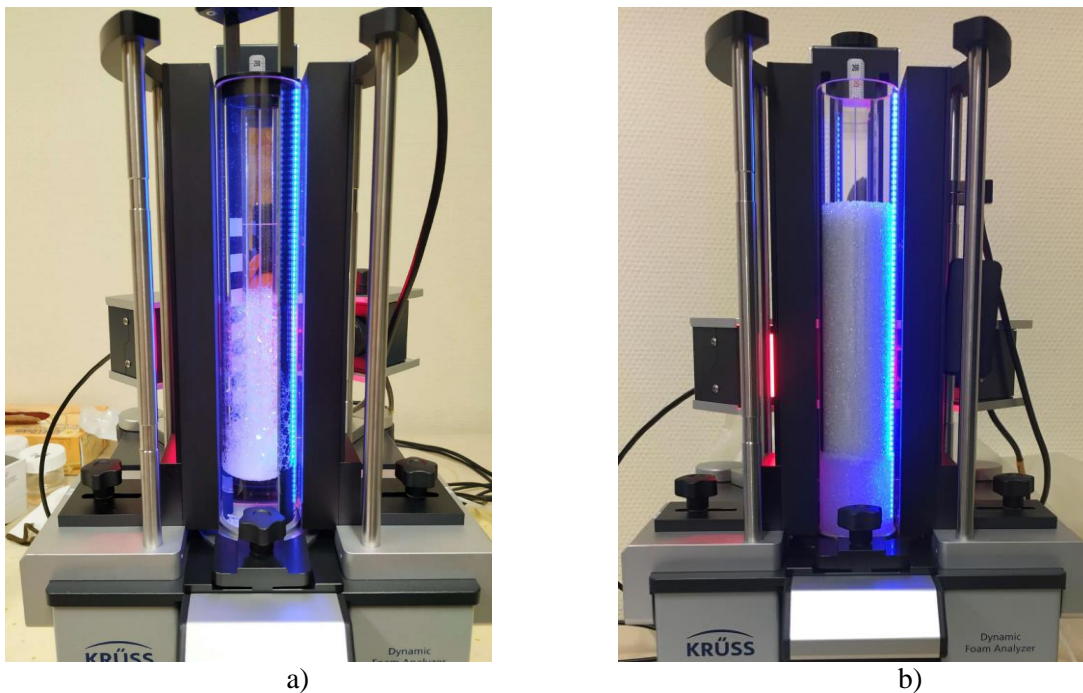


Fig. 1A Analysis of foam bubbles using dynamic foam analyzer (DFA-100, KRÜSS): a) in bulk form and b) in the porous medium (1 mm GB)

2A shows the change of structures in bulk foam and foam in 1 mm GB packing, where the mean bubble area (MBA) was compared after 60, 300, and 900 seconds. We observed that the bulk foam is less stable than foam in porous media. It is the consequence of the drainage process, which is greater for the bulk foam. For instance, the MBA of bulk foam doubled after 300 seconds, while the MBA of foam in 1 mm GB packing increased twice in 900 seconds, which was three times lower than the bulk foam. The bulk foam decays faster than the foam in porous media due to gravity drainage and gas diffusion, which tends to coalescence and coarsen average bubble size. While in porous media, the effect of gravity is small due to the short length scales within the bead-pack; therefore, the hydrostatic pressure differences are slight (Jones, et al., 2016). Jones et al. (2016) also found a correlation between apparent foam viscosity in porous media and the stability of foam in bulk form.

Moreover, from Fig. 2A, we can see that the shape of the bulk foam bubbles was changed from spherical to polyhedral over time, while the shape of the foam bubbles in porous media did not change, and it took the shape of pores to a greater degree.

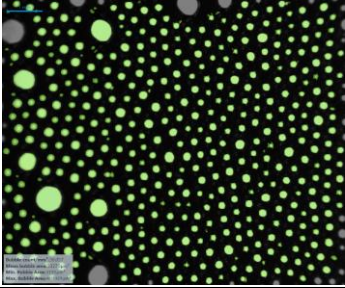
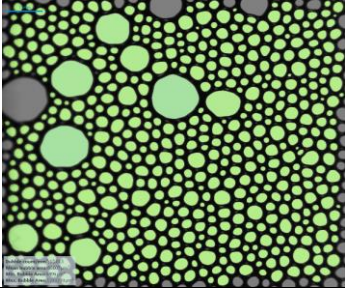
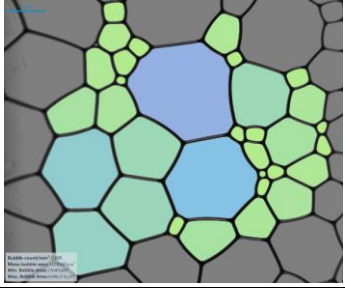
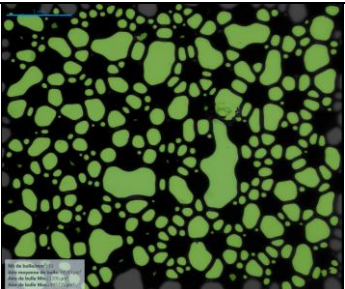
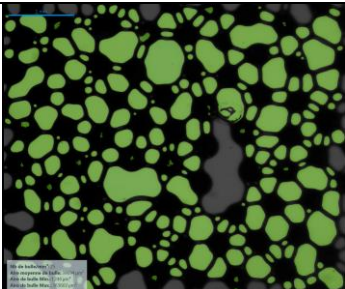
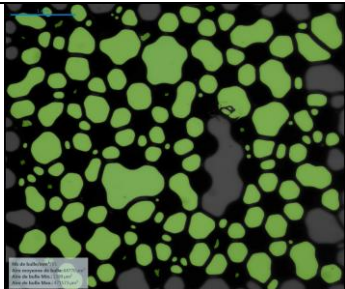
Time	60 sec	300 sec	900 sec
Bulk foam			
MBA _{bulk}	33,270 μm^2	66,607 μm^2	1,128,160 μm^2
1 mm GB packing			
MBA _{pm}	30,543 μm^2	39,694 μm^2	64,770 μm^2

Fig. 2A Change of foam structure as a function of time for bulk foam and foam in porous media (1 mm GB packing): liquid and solid phase in black, gas phase in color

In Fig. 3A, we plot the characteristic ratio of the bubble area (B_c) as a function of time, where B_c is the ratio of MBA_{pm} to MBA_{bulk} at the same time. In the beginning, the ratio is close to one. However, the values of B_c decrease with time showing that the variation of foam bubbles is much higher than for foam in the porous medium. Nevertheless, it must be noted that these experiments were conducted at ambient pressure in the static case. In addition, the height of the system exceeds 200 mm, which tends to increase bubble coalescence due to gravity drainage.

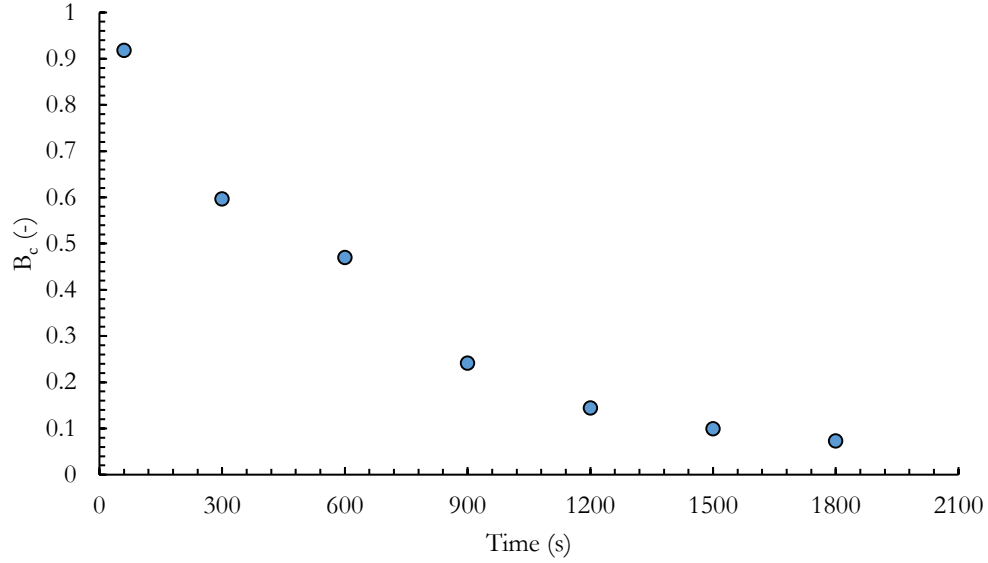


Fig. 3A The characteristic ratio of bubble area versus time ($B_c = MBA_{pm}/MBA_{bulk}$)

In the 1D column experiment, we expected the bubble change to be less than that detected by the foam analyzer. Because the foam was examined horizontally, therefore, the effect of gravity drainage was assumed to be weaker. Moreover, the foam in the 1D column flowed under a certain pressure, and according to the study by Holt et al. (1996), the foam strength (made of AOS surfactant) increases with increasing system pressure.

In our recent study (Omirebekov, et al., 2020), we compared the behavior of foams in 1 mm GB packing, where the foams were pre-generated in a 1 mm bead-pack and in a sand-pack used in this study. From the plot of apparent viscosity versus total flow rate, we noticed that the apparent foam viscosities vary greatly even at low flow rates, despite the long residence time of the foam in the column. Thus, it can be concluded that foam stability in confined environments is much longer than in bulk form. Nevertheless, we confirm that there was a small change in the size of the bubbles in the main column outlet. This should be studied with great care in future studies.

References

- Alvarez, J. M., Rivas, H. J. & Rossen, W. R., 2001. Unified Model for Steady-State Foam Behavior at High and Low Foam Qualities. *Society of Petroleum Engineers*.
- Aranda, R. et al., 2020. Experimental Study of Foam Flow in Highly Permeable Porous Media for Soil Remediation. *Transport in Porous Media*, Volume 134, p. 231–247.
- Ashoori, E., Marchesin, D. & Rossen, W. R., 2012. Multiple Foam States and Long-Distance Foam Propagation in EOR Displacements. *Society of Petroleum Engineers*.
- Auriault, J. L., 1991. Heterogeneous medium. Is an equivalent macroscopic description possible?. *International Journal of Engineering Science*, Volume 29, pp. 785-795.
- Bernard, G. G. & Holm, L. W., 1970. Model study of foam as a sealant for leaks in gas storage reservoirs. *Society of Petroleum Engineers Journal*, Volume 10, pp. 9-16.
- Berryman, J. G., 2005. Comparison of upscaling methods in poroelasticity and its generalizations. *Journal of Engineering Mechanics*, Volume 131, pp. 928-936.
- Bertin, H. J., Quintard, M. Y. & Castanier, L. M., 1998. Development of a Bubble-Population Correlation for Foam-Flow Modeling in Porous Media. *Society of Petroleum Engineers*.
- Briceno, M. I. & Joseph, D. D., 2003. Self-lubricated transport of aqueous foams in horizontal conduits. *International journal of multiphase flow*, Volume 29, pp. 1817-1831.
- Carman, P. C., 1997. Fluid flow through granular beds. *Chemical Engineering Research and Design*, Volume 75, pp. S32 - S48.
- Chatzis, I. & Morrow, N. R., 1984. Correlation of capillary number relationships for sandstone. *Society of Petroleum Engineers Journal*, Volume 24, p. 555–562.
- Chauveteau, G., 1982. Rodlike polymer solution flow through fine pores: influence of pore size on rheological behavior. *Journal of Rheology*, Volume 26, pp. 111-142.
- Chauveteau, G. & Zaitoun, A., 1981. *Basic rheological behavior of xanthan polysaccharide solutions in porous media: effects of pore size and polymer concentration*. s.l., s.n., pp. 197-212.
- Chen, Y. et al., 2014. Switchable nonionic to cationic ethoxylated amine surfactants for CO₂ enhanced oil recovery in high-temperature, high-salinity carbonate reservoirs. *SPE journal*, Volume 19, pp. 249-259.
- Chevalier, T. et al., 2013. Darcy's law for yield stress fluid flowing through a porous medium. *Journal of Non-Newtonian Fluid Mechanics*, Volume 195, pp. 57-66.
- Chevalier, T. et al., 2014. Breaking of non-Newtonian character in flows through a porous medium. *Physical Review E*, Volume 89, p. 023002.

- Choi, Y. J., Kim, Y.-J. & Nam, K., 2009. Enhancement of aerobic biodegradation in an oxygen-limiting environment using a saponin-based microbubble suspension. *Environmental pollution*, Volume 157, pp. 2197-2202.
- Christopher, R. H. & Middleman, S., 1965. Power-law flow through a packed tube. *Industrial & Engineering Chemistry Fundamentals*, Volume 4, pp. 422-426.
- Cohen-Addad, S., Höhler, R. & Pitois, O., 2013. Flow in Foams and Flowing Foams. *Annual Review of Fluid Mechanics*, Volume 45, pp. 241-267.
- Coussot, P., 2005. *Rheometry of Pastes, Suspensions, and Granular Materials: Applications in Industry and Environment*. s.l.:Wiley.
- Cserháti, T., Forgács, E. & Oros, G., 2002. Biological activity and environmental impact of anionic surfactants. *Environment International*, Volume 28, pp. 337-348.
- Darby, R., Darby, R. & Chhabra, R. P., 2001. *Chemical engineering fluid mechanics, revised and expanded*. s.l.:CRC Press.
- Darcy, H. P. G., 1856. *Les Fontaines publiques de la ville de Dijon. Exposition et application des principes à suivre et des formules à employer dans les questions de distribution d'eau, etc.* s.l.:V. Dalamont.
- Denkov, N. D., Subramanian, V., Gurovich, D. & Lips, A., 2005. Wall slip and viscous dissipation in sheared foams: Effect of surface mobility. *Colloids and Surfaces A: Physicochemical and Engineering Aspects*, Volume 263, pp. 129-145.
- Denkov, N. D. et al., 2009. The role of surfactant type and bubble surface mobility in foam rheology. *Soft Matter*, 5(18), pp. 3389-3408.
- Dicksen, T., Hirasaki, G. J. & Miller, C. A., 2002. Conditions for Foam Generation in Homogeneous Porous Media. *Society of Petroleum Engineers*.
- Ding, M. & Kantzas, A., 2007. Capillary number correlations for gas-liquid systems. *Journal of Canadian Petroleum Technology*, Volume 46.
- Dollet, B. & Raufaste, C., 2014. Rheology of aqueous foams. *Comptes Rendus Physique*, Volume 15, pp. 731-747.
- Ettinger, R. A., Radke, C. J. & others, 1992. Influence of texture on steady foam flow in Berea sandstone. *SPE reservoir engineering*, Volume 7, p. 83-90.
- Falls, A. H., Musters, J. J. & Ratulowski, J., 1989. The apparent viscosity of foams in homogeneous bead packs. *SPE (Society of Petroleum Engineers) Reserv. Eng.; (United States)*, 5. Volume 4:2.

- Farajzadeh, R., Andrianov, A., Bruining, H. & Zitha, P. L. J., 2009. Comparative Study of CO₂ and N₂ Foams in Porous Media at Low and High Pressure–Temperatures. *Industrial & Engineering Chemistry Research*, Volume 48, pp. 4542-4552.
- Fletcher, A. J. P. et al., 1991. *Measurements of polysaccharide polymer properties in porous media*. s.l., s.n.
- Friedmann, F., Chen, W. H. & Gauglitz, P. A., 1991. Experimental and simulation study of high-temperature foam displacement in porous media. *SPE (Society of Petroleum Engineers) Reservoir Engineering; (United States)*, 2. Volume 6:1.
- Friedmann, F. & Jensen, J. A., 1986. *Some parameters influencing the formation and propagation of foams in porous media*. s.l., s.n.
- Gardiner, B. S., Dlugogorski, B. Z. & Jameson, G. J., 1998. Rheology of fire-fighting foams. *Fire Safety Journal*, Volume 31, p. 61–75.
- Gardiner, B. S., Dlugogorski, B. Z. & Jameson, G. J., 1999. Prediction of pressure losses in pipe flow of aqueous foams. *Industrial & engineering chemistry research*, Volume 38, p. 1099–1106.
- Gauglitz, P. A., Friedmann, F., Kam, S. I. & Rossen, W. R., 2002. Foam generation in homogeneous porous media. *Chemical Engineering Science*, Volume 57, pp. 4037-4052.
- Herschel, W. H. & Bulkley, R., 1926. Konsistenzmessungen von gummi-benzollösungen. *Kolloid-Zeitschrift*, Volume 39, pp. 291-300.
- Herzhaft, B., 1999. Rheology of Aqueous Foams: a Literature Review of some Experimental Works. *Oil & Gas Science and Technology*, 7, Volume Vol. 54 (1999), pp. 587-596.
- Hirasaki, G. J. & Lawson, J. B., 1985. Mechanisms of Foam Flow in Porous Media: Apparent Viscosity in Smooth Capillaries. *Society of Petroleum Engineers*.
- Hirasaki, G. J. et al., 1997. Surfactant/Foam Process for Aquifer Remediation. *Society of Petroleum Engineers*, 1.
- Hirasaki, G. J. & Pope, G. A., 1974. Analysis of factors influencing mobility and adsorption in the flow of polymer solution through porous media. *Society of Petroleum Engineers Journal*, Volume 14, pp. 337-346.
- Hohler, R. & Cohen-Addad, S., 2005. Rheology of liquid foam. *Journal of Physics: Condensed Matter*, Volume 17.
- Holt, T., Vassenden, F. & Svorstol, I., 1996. *Effects of pressure on foam stability; Implications for foam screening*. s.l., s.n.
- Idris, Z. et al., 2004. Microstructural effects on the flow law of power-law fluids through fibrous media. *Modelling and Simulation in Materials Science and Engineering*, Volume 12, p. 995.

- Jones, S. A. et al., 2016. Surfactant screening for foam EOR: Correlation between bulk and core-flood experiments. *Colloids and Surfaces A: Physicochemical and Engineering Aspects*, Volume 500, p. 166–176.
- Kam, S. I., 2008. Improved mechanistic foam simulation with foam catastrophe theory. *Colloids and Surfaces A: Physicochemical and Engineering Aspects*, Volume 318, pp. 62-77.
- Katgert, G., Tighe, B. P. & Hecke, M., 2013. The jamming perspective on wet foams. *Soft Matter*, 9(41), pp. 9739-9746.
- Khan, S. A., Schnepfer, C. A. & Armstrong, R. C., 1988. Foam Rheology: III. Measurement of Shear Flow Properties. *Journal of Rheology*, Volume 32, pp. 69-92.
- Kovscek, A. R., Chen, Q. & Gerritsen, M., 2010. Modeling Foam Displacement With the Local-Equilibrium Approximation: Theory and Experimental Verification. *Society of Petroleum Engineers*.
- Kovscek, A. R. & Radke, C. J., 1994. Fundamentals of foam transport in porous media. *ACS Advances in Chemistry Series*, Volume 242, pp. 115-164.
- Kovscek, A. R., Tadeusz, W. P. & Radke, C. J., 1997. Mechanistic foam flow simulation in heterogeneous and multidimensional porous media. *SPE Journal*, Volume 2, pp. 511-526.
- Kozeny, J., 1927. Uber kapillare leitung der wasser in boden. *Royal Academy of Science, Vienna, Proc. Class I*, Volume 136, pp. 271-306.
- Kraynik, A. M., 1988. Foam Flows. *Annual Review of Fluid Mechanics*, Volume 20, pp. 325-357.
- Langevin, D., 2017. Aqueous foams and foam films stabilised by surfactants. Gravity-free studies. *Comptes Rendus Mécanique*, Volume 345, pp. 47-55.
- Larmignat, S., Vanderpool, D., Lai, H. K. & Pilon, L., 2008. Rheology of colloidal gas aphrons (microfoams). *Colloids and Surfaces A: Physicochemical and Engineering Aspects*, Volume 322, pp. 199-210.
- Larry, W. L., Russell, J., Bill, R. & Gary, P., 1986. *Fundamentals of Enhanced Oil Recovery*. s.l.:Society of Petroleum Engineers.
- Larson, R. G., 1999. *The Structure and Rheology of Complex Fluids*. s.l.:New York: Oxford University Press.
- Liu, A. J. & Nagel, S. R., 1998. Jamming is not just cool any more. *Nature*, Volume 396, pp. 21-22.
- Macosko, C. W., 1994. *Rheology: Principles, Measurements, and Applications*. s.l.:Wiley-VCH.
- Maire, J., Davarzani, H., Colombano, S. & Fatin-Rouge, N., 2019. Targeted delivery of hydrogen for the bioremediation of aquifers contaminated by dissolved chlorinated compounds. *Environmental Pollution*, Volume 249, pp. 443-452.

- Ma, K. et al., 2015. Modeling Techniques for Foam Flow in Porous Media. *Society of Petroleum Engineers*, 6. Volume 20.
- Marsden, S. S., Eerligh, J. P., Albrecht, R. A. & David, A., 1967. *Use of foam in petroleum operations*. s.l., s.n.
- Marze, S., Guillermic, R. M. & Saint-Jalmes, A., 2009. Oscillatory rheology of aqueous foams: surfactant, liquid fraction, experimental protocol and aging effects. *Soft Matter*, 5(9), pp. 1937-1946.
- Marze, S., Saint-Jalmes, A. & Langevin, D., 2008. Aqueous foam slip and shear regimes determined by rheometry and multiple light scattering. *Journal of rheology*, Volume 52, p. 1091.
- Myers, T. J. & Radke, C. J., 2000. Transient Foam Displacement in the Presence of Residual Oil: Experiment and Simulation Using a Population-Balance Model. *Industrial & Engineering Chemistry Research*.
- Omirebekov, S., Davarzani, H. & Ahmadi-Senichault, A., 2020. Experimental Study of Non-Newtonian Behavior of Foam Flow in Highly Permeable Porous Media. *Industrial & Engineering Chemistry Research*.
- Orgéas, L., Geindreau, C., Auriault, J.-L. & Bloch, J.-F., 2007. Upscaling the flow of generalised Newtonian fluids through anisotropic porous media. *Journal of Non-Newtonian Fluid Mechanics*, Volume 145, pp. 15-29.
- Orgéas, L. et al., 2006. Modelling the flow of power-law fluids through anisotropic porous media at low-pore Reynolds number. *Chemical engineering science*, Volume 61, pp. 4490-4502.
- Osterloh, W. T. & Jante Jr, M. J., 1992. *Effects of gas and liquid velocity on steady-state foam flow at high temperature*. s.l., s.n.
- Otsubo, Y. & Prud'homme, R. K., 1994. Effect of drop size distribution on the flow behavior of oil-in-water emulsions. *Rheologica Acta*, Volume 33, pp. 303-306.
- Otsubo, Y. & Prud'homme, R. K., 1994. Rheology of oil-in-water emulsions. *Rheologica acta*, Volume 33, pp. 29-37.
- Ovarlez, G., Krishan, K. & Cohen-Addad, S., 2010. Investigation of shear banding in three-dimensional foams. *EPL - Europhysics Letters*, Volume 91, p. 68005.
- Ovarlez, G. et al., 2008. Wide-gap Couette flows of dense emulsions: Local concentration measurements, and comparison between macroscopic and local constitutive law measurements through magnetic resonance imaging. *Physical Review E : Statistical, Nonlinear, and Soft Matter Physics*, 9, Volume 78, p. 036307.
- Papanastasiou, T. C., 1987. Flows of Materials with Yield. *Journal of Rheology*, Volume 31, pp. 385-404.

- Papanicolau, G., Bensoussan, A. & Lions, J.-L., 1978. *Asymptotic Analysis for Periodic Structures*. s.l.:North Holland.
- Paria, S., 2008. Surfactant-enhanced remediation of organic contaminated soil and water. *Advances in Colloid and Interface Science*, Volume 138, pp. 24-58.
- Persoff, P. et al., 1991. A Laboratory Investigation of Foam Flow in Sandstone at Elevated Pressure.. *Society of Petroleum Engineers.*, 8.
- Princen, H. M. & Kiss, A. D., 1989. Rheology of foams and highly concentrated emulsions: IV. An experimental study of the shear viscosity and yield stress of concentrated emulsions. *Journal of Colloid and Interface Science*, Volume 128, pp. 176-187.
- Prud'homme, R. K. & Khan, S. A., 2017. *FOAMS. Theory, Measurements, and Applications*. s.l.:Routledge.
- Quintard, M. & Whitaker, S., 1993. Transport in ordered and disordered porous media: volume-averaged equations, closure problems, and comparison with experiment. *Chemical Engineering Science*, Volume 48, pp. 2537-2564.
- Quintard, M. & Whitaker, S., 1994. Transport in ordered and disordered porous media III: Closure and comparison between theory and experiment. *Transport in Porous Media*, Volume 15, pp. 31-49.
- Ransohoff, T. C. & Radke, C. J., 1988. Mechanisms of Foam Generation in Glass-Bead Packs. *Society of Petroleum Engineers*.
- Rodríguez de Castro, A., 2019. Extending Darcy's law to the flow of yield stress fluids in packed beds: Method and experiments. *Advances in water resources*, Volume 126, pp. 55-64.
- Rossen, W. R. & Gauglitz, P. A., 1990. Percolation theory of creation and mobilization of foams in porous media. *AIChE Journal*, Volume 36, pp. 1176-1188.
- Rossen, W. R. & Wang, M. W., 1999. Modeling foams for acid diversion. *SPE journal*, Volume 4, pp. 92-100.
- Saint-Jalmes, A. & Durian, D. J., 1999. Vanishing elasticity for wet foams: Equivalence with emulsions and role of polydispersity. *Journal of Rheology*, Volume 43, pp. 1411-1422.
- Sanchez-Palencia, E., 1980. *Non-Homogeneous Media and Vibration Theory Lecture Notes in Physics*. s.l.:Springer-Verlag Berlin Heidelberg.
- Sander, R., 1999. *Compilation of Henry's law constants for inorganic and organic species of potential importance in environmental chemistry*. s.l.:Max-Planck Institute of Chemistry, Air Chemistry Department Mainz, Germany.
- Satter, A. & Iqbal, G. M., 2015. *Reservoir engineering: the fundamentals, simulation, and management of conventional and unconventional recoveries*. s.l.:Gulf Professional Publishing.

- Stauffer, C. E., 1965. The measurement of surface tension by the pendant drop technique. *The journal of physical chemistry*, Volume 69, pp. 1933-1938.
- Svab, M., Kubal, M., Müllerova, M. & Raschman, R., 2009. Soil flushing by surfactant solution: Pilot-scale demonstration of complete technology. *Journal of Hazardous Materials*, Volume 163, pp. 410-417.
- Talmage, S. S., 1994. *Environmental and human safety of major surfactants: alcohol ethoxylates and alkylphenol ethoxylates*. s.l.:CRC Press.
- Tcholakova, S. et al., 2008. Theoretical model of viscous friction inside steadily sheared foams and concentrated emulsions. *Phys. Rev. E*, 7, 78(1), p. 011405.
- Tuvell, M. E. et al., 1978. AOS --- An anionic surfactant system: Its manufacture, composition, properties, and potential application. *Journal of the American Oil Chemists' Society*, 01 1, Volume 55, pp. 70-80.
- Valko, P. & Economides, M. J., 1992. Volume equalized constitutive equations for foamed polymer solutions. *Journal of Rheology*, Volume 36, p. 1033–1055.
- Vassenden, F. & Holt, T., 2000. Experimental Foundation for Relative Permeability Modeling of Foam. *Society of Petroleum Engineers*.
- Wang, X.-H., Jia, J.-T., Liu, Z.-F. & Jin, L.-D., 2014. Derivation of the Darcy-scale filtration equation for power-law fluids with the volume averaging method. *Journal of Porous Media*, Volume 17.
- Whitaker, S., 1999. *The Method of Volume Averaging*. s.l.:Springer Netherlands.
- Woods, J. K. et al., 2003. Creeping flows of power-law fluids through periodic arrays of elliptical cylinders. *Journal of non-newtonian fluid mechanics*, Volume 111, pp. 211-228.
- Zeng, Y. et al., 2016. Role of gas type on foam transport in porous media. *Langmuir*, Volume 32, pp. 6239-6245.
- Zitha, P., Chauveteau, G. & Zaitoun, A., 1995. *Permeability~ Dependent Propagation of Polyacrylamides Under Near-Wellbore Flow Conditions*. s.l., s.n.